Zero field NMR and NQR

D. B. Zax,[a] A. Bielecki, K. W. Zilm,[b] A. Pines, and D. P. Weitekamp
Department of Chemistry, University of California, Berkeley, and Materials and Molecular Research Division, Lawrence Berkeley Laboratory, Berkeley, California 94720

(Received 14 June 1985; accepted 7 August 1985)

Methods are described and demonstrated for detecting the coherent evolution of nuclear spin observables in zero magnetic field with the full sensitivity of high field NMR. The principle motivation is to provide a means of obtaining solid state spectra of the magnetic dipole and electric quadrupole interactions of disordered systems without the line broadening associated with random orientation with respect to the applied magnetic field. Comparison is made to previous frequency domain and high field methods. A general density operator formalism is given for the experiments where the evolution period is initiated by a sudden switching to zero field and is terminated by a sudden restoration of the field. Analytical expressions for the signals are given for a variety of simple dipolar and quadrupolar systems and numerical simulations are reported for up to six coupled spin-1/2 nuclei. Experimental results are reported or reviewed for ^{1}H, ^{2}D, ^{7}Li, ^{13}C, and ^{27}Al nuclei in a variety of polycrystalline materials. The effects of molecular motion and bodily sample rotation are described. Various extensions of the method are discussed, including demagnetized initial conditions and correlation by two-dimensional Fourier transformation of zero field spectra with themselves or with high field spectra.

I. INTRODUCTION

A. Basic physical picture

The static magnetic field B_0 plays several distinct roles in the usual nuclear magnetic resonance (NMR) experiment. When the sample is placed in the field, a net alignment of the spins along the field axis is established with a time constant T_1, and attains an asymptotic value which in the high temperature, or Curie law, limit is proportional to the field. When the spins are coherently perturbed from this equilibrium, they precess at their Larmor frequencies ($\omega_0 = \gamma B_0$), which are also proportional to the field. Thus, the strength of the field during coherent precession will determine the resolution with which a Zeeman interaction (such as the chemical shift or Knight shift) can be measured. Field strength figures also in the signal-to-noise ratio, since the induced voltage in the detection coil is proportional to frequency and initial magnetization. It is, therefore, not surprising that the tendency of modern NMR spectroscopists is to work at the highest magnetic fields available.

Because the application of a magnetic field is necessary to measure Zeeman terms and to obtain a useable signal strength, it is easy to overlook the fact that the information content of the spectrum is greatly altered by the loss of isotropic spatial symmetry caused by the application of an external field, just as the application of an x-ray or neutron beam in diffraction experiments establishes a unique direction in space. Consider, for example, the information carried in the couplings between the magnetic dipoles of nearby spins, or between the molecular electric field gradient and the nuclear quadrupole moment of a nucleus with spin $I>1$. These couplings may be viewed for simplicity as local fields which add vectorially to any applied field. If the applied field is much larger in magnitude, then to a good approximation only the components of the local fields parallel to it are measureable. Molecules with different fixed orientations contribute different local fields in this direction and thus exhibit different energy levels and transition frequencies, as illustrated in Fig. 1 for the simple case of two identical spin-1/2 nuclei. The magnitude of the spectral splitting $\Delta\omega$ for two such spins i and j depends on both r_{ij}, the distance between these two spins, and θ_{ij}, the angle between the internuclear vector and the applied field

$$\Delta\omega \sim (3\cos^2\theta_{ij} - 1)/r_{ij}^3 . \quad (1)$$

This angular dependence can be informative in those cases where the distribution of molecular orientations with respect to the laboratory is not known. For a single crystal, spectra obtained at different sample orientations may be analyzed to give the angular relationship between the crystal axes and the molecular axes.[1] In partially oriented systems, such as stretched polymers or some liquid crystals,[2] the high field spectrum provides information on the domain structure and orientational distribution within domains.

Here we focus on the more commonly encountered situation where the sample consists of a large number of spin systems which differ only in their orientation referenced to the laboratory frame and where all possible orientations are equally represented. Such an ensemble is characteristic of powders of crystalline substances, species adsorbed on powders, liquid crystals with random directors, or amorphous systems such as glasses and many polymers and semiconductors. In sufficiently simple spin systems such a distribution gives rise to well known high-field powder patterns.[3] Figure 1 at the bottom shows the prototypical example, the

[a] Current address: Isotope Division, Weizmann Institute of Science, Rehovot 76100, Israel.
[b] Current address: Department of Chemistry, Yale University, New Haven, Connecticut 06511.

 0021-9606/85/224877-29$02.10

"Pake pattern"[4] which arises from two dipolar-coupled spin-1/2 nuclei, and which corresponds to a weighted sum over all possible orientations of the two nuclei.

Figure 2 shows experimental high field NMR spectra of the water ^1H nuclei in solid $Ba(ClO_3)_2 \cdot H_2O$. Because the water molecules are well isolated from one another, the spectrum is dominated by interactions between a single pair of ^1H nuclei. Figure 2 (top) shows the spectrum of a single crystal sample at a randomly chosen orientation. It shows the inherent resolution for a typical crystallite in a powder. As all of the signal is concentrated in a small number of lines, the signal-to-noise ratio is good and an analysis of the observed absorption pattern straightforward. But no single spectrum contains sufficient information to completely characterize the couplings. A number of spectra at different orientations are required to separate the distance dependence from the angular factor. Figure 2 (bottom) is the high field powder pattern arising from a polycrystalline sample. In this simple case, the positions of observed singularities allow a determination of the components of the local fields more readily

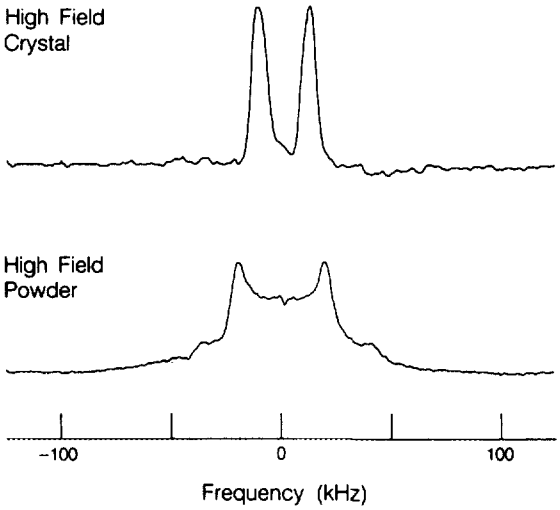

FIG. 2. Experimental high field ^1H NMR spectra of $Ba(ClO_3)_2 \cdot H_2O$. Top: single crystal spectrum. All of the spectral intensity is concentrated in a pair of lines as all the sites in the unit cell have $\mathbf{r}_{ij}$, the interproton vector, parallel. The magnitude of the observed splitting depends on the internuclear distance and the orientation of the crystal in the field. Bottom: powder spectrum. This simple spectrum can be directly interpreted as in Fig. 1.

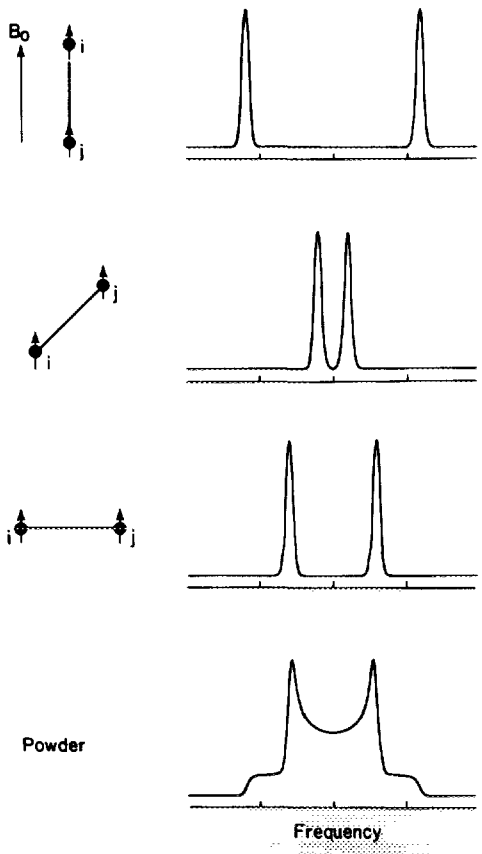

FIG. 1. Simulated high field dipolar spectra for two equivalent spins i and j, convoluted with a Gaussian function to simulate the effects of near neighbors. From top to bottom: Simulations for the specific orientations of the internuclear vector pictured at left. The magnetic field is assumed large and oriented vertically. θ_{ij} is the angle between the applied field and the internuclear vector. Spectra are shown for $\theta_{ij} = 0°$, 48°, and 90°. At bottom, we show the powder pattern, which is the sum over all values of θ_{ij} weighted by their probability. In this simple case, the singularities in the powder pattern (peaks and shoulders) can be identified as arising from specific orientations (i.e., the 90° and 0° orientations) and the spectrum is easily interpreted. The internuclear distance is given by $\langle r^{-3} \rangle = 2\Delta\omega/3\gamma^2\hbar$, where $\Delta\omega$ is the frequency difference between the two peaks.

than if only single crystals were available, since the distribution of orientations (i.e., all possible rotations) is known. The accuracy with which this determination can be made will, in any particular case, depend on the broadening of the ideal discontinuous powder line shape by irreversible relaxation or, more often, by unresolved couplings to distant spins. Given the wide initial distribution of frequencies with which this broadening may be convoluted, the signal-to-noise ratio may be lowered and useful information present in the spectrum lost.

Even where only a few spins are coupled one to another, the spectrum rapidly degenerates into a nearly featureless broad band of absorption frequencies. An example involving groups of four spins in a powder is the high field proton spectrum of polycrystalline 1,2,3,4-tetrachloronaphthalene bis (hexachlorocyclopentadiene) adduct, shown in Fig. 3. We will return to a structural analysis of this system based on zero field NMR in Sec. III B 1.

Ideally, then, one would prefer for structural studies a crystal-like spectrum of discrete transitions without the requirement of a single crystal and a rotation pattern analysis. The desired spectrum is just what one would observe in the absence of a magnetic field. In zero field, all spins experience only their mutual local fields and all molecular or crystalline orientations in space are spectroscopically equivalent; i.e., only a finite number of identical transition frequencies are allowed. Such a zero field spectrum of a polycrystalline sample of $Ba(ClO_3)_2 \cdot H_2O$ is shown in Fig. 4. It has the resolution of the single crystal spectrum of Fig. 2 but is obtained from a powder sample.

The present paper is a more complete presentation of our results with the new method[5] of Fourier transform time domain zero field NMR and NQR, which achieves time domain zero field spectroscopy with the sensitivity of high field methods. It is a Fourier transform analog of the field cycling, frequency domain experiments of Ramsey and Pound, An-

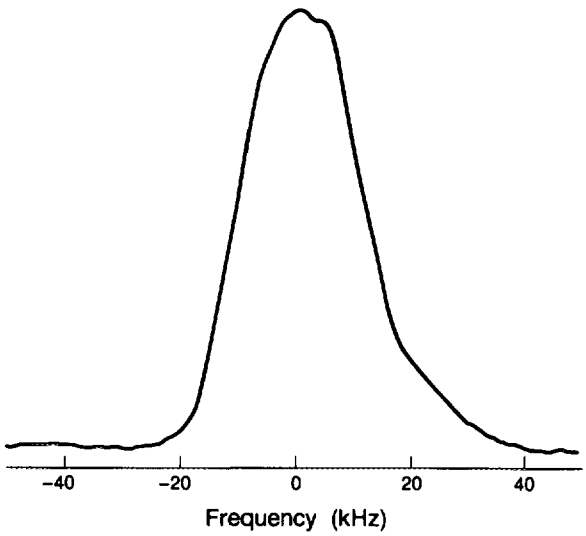

FIG. 3. High field spectrum of polycrystalline 1, 2, 3, 4-tetrachloronaphthalene bis(hexachlorocyclopentadiene) adduct. Like most dipolar powder patterns, little structure is resolved, even though only a small number of spins (4) are strongly coupled together, and sets of these spins are relatively isolated from others.

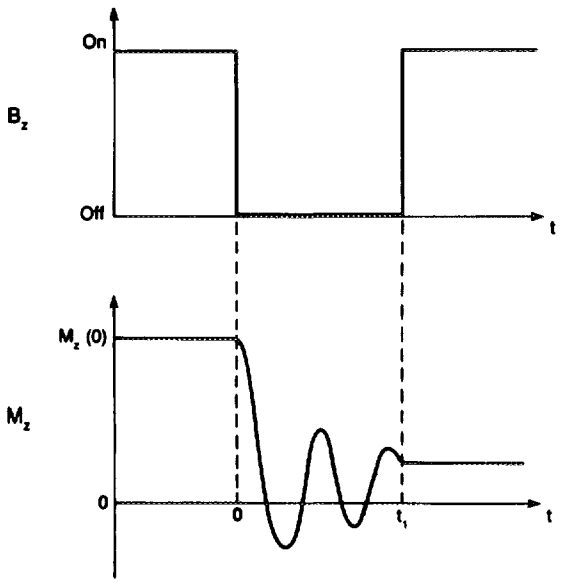

FIG. 5. Idealized representation of the time domain field cycling experiment. Top, the magnetic field profile as a function of time. Bottom, the corresponding profile of the nuclear spin magnetization. In high field, an equilibrium magnetization is established in a time $\sim T_1$ (not shown). The magnetic field is instantaneously shut off. The magnetization begins to oscillate and is allowed to evolve for a time t_1. The magnetic field is instantaneously reapplied and evolution is terminated. The amplitude of the evolved magnetization is then sampled by standard high field NMR techniques. The field cycle is then repeated for a number of equally spaced values of t_1. The sequence of values of $M_z(t_1)$ constitute the zero field free induction decay, and Fourier transformation yields the zero field spectrum.

derson, Redfield, Hahn, and others.[6–10] An idealized timing diagram for the basic experiment is shown in Fig. 5. The sample starts in a high magnetic field where the spin system approaches the equilibrium magnetization with a time constant T_1. The field applied to the polarized sample is then rapidly decreased. Practical timing requirements are discussed in Sec. VI A 1. The novel feature of this field cycling experiment is that the final approach to zero takes place sufficiently suddenly so that during the transition the spins are unable to appreciably realign. Rather, they find themselves with a common direction and magnitude of polarization appropriate to equilibrium in the previous high external field, yet only the weaker local fields remain. The spins respond by precessing about these local fields. Thus the collective spin magnetization begins coherent oscillations which are allowed to proceed, in the local fields alone, for an evolution period t_1. These oscillations cannot themelves be sensitively observed using normal Faraday-law NMR detectors due to their low frequency. Instead, their evolution is terminated and stored by the sudden reapplication of an external field. Any further free precession is about the direction of the applied field. That magnetization remaining parallel to the applied field is persistent for times short compared to T_1. With the high field restored, standard rf methods are used to detect this surviving magnetization during the detection period t_2. This sequence is repeated for increasing values of the zero field period t_1 and the measured signal is observed to oscillate and decay. Fourier transformation yields the spectrum of these oscillations, which displays the frequencies characteristic of the spin system in the absence of any external fields, but detected by means of high field NMR techniques. The indirect detection of an NMR spectrum evolving under one Hamiltonian by its effect on the spectrum which is observed during a second time period is the basis of all two-dimensional NMR techniques.[11] In order to distinguish this basic method from variants which have appeared elsewhere[12] and which will be discussed below, we label it zero field NMR by sudden switching.

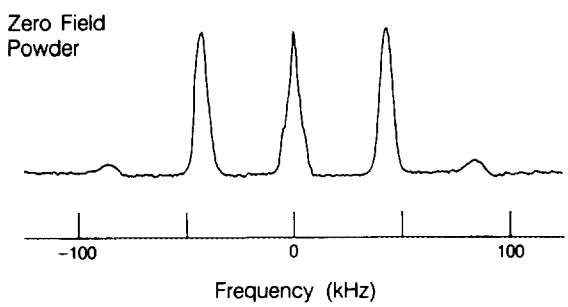

FIG. 4. Zero field NMR spectrum of polycrystalline $Ba(ClO_3)_2 \cdot H_2O$. The intensity is concentrated in a small number of sharp bands. Like the simple two-spin Pake pattern, the frequencies of the lines are directly interpretable. The high frequency ($\pm \sim 42$ kHz) lines appear at exactly the position of the shoulders in the high field powder pattern (Fig. 2). The frequency of these lines correspond to $\langle r^{-3} \rangle^{-1/3} = 1.62 \pm 0.01$ Å.

Figure 4 is the ^1H zero field spectrum of the polycrystalline sample of $Ba(ClO_3)_2 \cdot H_2O$ whose high field spectrum is shown in Fig. 2 at the bottom. To a first approximation it can be analyzed, like the high field spectrum, as due to isolated two-spin systems. The prominent pair of lines at $\pm \sim 42$ kHz represents the precession in the local field of that component of magnetization which at $t_1 = 0$ lies perpendicular to the internuclear vector. The central line corresponds to the component which lies along the internuclear vector and experiences no torque. Proton pairs oriented along the field

axis as in Fig. 1 (top) contribute only to the central line while those perpendicular to the field (Fig. 1, second from bottom) contribute only to the outer pair of lines. Other orientations contribute to both features. The precession frequency, however, is orientation independent and gives rise to discrete spectral splittings in a powder rather than the continuum of Fig. 2 (bottom). For this two-spin system, the zero field splitting is identical to the maximum pair separation in high field, as may be seen by comparison to the powder pattern of Fig. 2. The internuclear distance is given directly without any need to separate it from an angular factor. A fuller analysis of this spectrum is given in Sec. II C.

In Sec. III we present our results for zero field NMR studies on more complex systems, such as the four-spin system of Fig. 3. Here the resolution advantage of the zero field powder spectrum over the high field powder spectrum becomes more crucial. The important point is that, whatever the spin system, the local fields alone determine the spectral frequencies. The molecular orientation enters only in line intensities, and powder average is easily calculated by the procedure described in Sec. II B.

B. Relationship to other zero field methods

The resolution advantage of zero field studies for orientationally disordered samples is well known from related magnetic resonance methods. In zero field ESR[13] and pure NQR[14] the polarization comes from the equilibrium population differences between zero field levels. This is typically sufficient when these splittings are greater than a few MHz. Both frequency and time domain methods are used in such studies. In the unusually favorable cases of solid H_2[15] and polarized Cu,[16] continuous wave (cw) zero field NMR signals were seen from spin ordering in the local fields alone, at lower frequencies. Observation of time domain zero field signals has also been made with the method of perturbed angular correlations[17] which is based on coincidence measurements of the angular distribution of radioactive emissions. The high sensitivity often makes a polarizing field unnecessary.

The time domain methods of the present work are complementary, being appropriate to more general systems where the small size of the couplings makes the sensitivity of a pure zero field experiment (in the absence of exceedingly low temperatures or otherwise unusually large nuclear polarizations) inadequate. This is always the case for spin 1/2 nuclei, where the dipolar spectrum is nearly always below 100 kHz, and for quadrupolar nuclei with small nuclear quadrupole moments, such as ^{2}D, ^{6}Li, ^{7}Li, and ^{23}Na. It is also useful for nuclei with larger quadrupole moments (^{14}N, ^{17}O, and ^{27}Al) in environments of near tetrahedral or higher symmetry, where the energy splittings due to the quadrupolar interaction may be less than 1 MHz. The method should also be applicable to zero field ESR; i.e., the measurement of hyperfine couplings in powder samples in zero field.

The idea of increasing the signal-to-noise ratio of zero field spectra by cycling from and to a high polarizing and detection field, has been used previously in a number of frequency domain experiments. If the sample is brought to near-zero field rapidly enough to prevent equilibration of the spin polarization with the lattice but slowly enough not to induce transients the demagnetization of the spin reservoir is adiabatic. In zero field a weak audio or rf irradiation is made. The depolarization or heating of the spin system is monitored with high field methods after adiabatic remagnetization. Repetition of the experiment with different irradiation frequencies provides a zero field spectrum. From the start[6] it was recognized that in these experiments the low field resonances of one spin species may appear as a magnetization loss in the high field signal of a second species. This concept of indirect detection by polarization transfer[8,9] has been developed into a variety of high sensitivity, frequency domain NQR methods.[10]

All frequency domain experiments require care if power broadening is to be avoided. Signal intensity is maximized at power levels that distort the spectrum. A more serious difficulty for the indirect detection NQR methods is that low frequency transitions of the quadrupolar nucleus may fall in the region where direct absorption by the detected species masks the heating through polarization transfer. These low frequency lines are only rarely accessible.[18] This is of particular importance for spin 1 nuclei (^{2}D and ^{14}N), where low frequency transitions may prove essential to the assignment of the signals.

The present experiments avoid both problems since

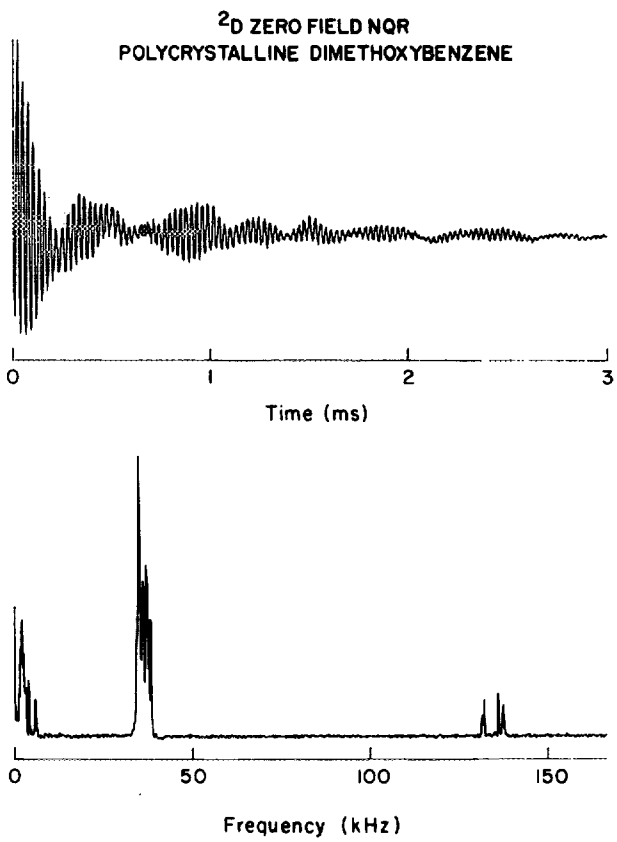

FIG. 6. Top: zero field NQR free induction decay from polycrystalline sample of perdeuterated 1,4-dimethoxybenzene. The time domain evolution is sampled at 3 μs intervals for a total of 3 ms. The magnetization evolves at all the frequencies characteristic of the Hamiltonian in the absence of an applied field. Bottom: Fourier transform of the zero field free induction decay at top.

there are no applied fields during the zero field evolution time. This allows for extremely high resolution and enhanced sensitivity in the detection of low frequency NQR lines, as illustrated in Fig. 6 and further discussed in Sec. IV B. The figure shows the zero field ^{2}D spectrum of perdeuterated polycrystalline 1,4-dimethoxybenzene, obtained by zero field NQR with sudden switching. Working in the time domain also makes possible a variety of experiments incorporating two-dimensional Fourier transformation,[11] some of which are presented in Secs. VI B and VII. As we discuss in Sec. VII C 2, it is possible to combine the sensitivity advantage of the indirect methods for observation of rare nuclear spins with our Fourier transform method. The method of Fig. 5, i.e., sudden switching of B_0, is only the simplest of a number of related methods. (A similar technique has been used to measure the strength of the earth's magnetic field[19].) This paper also describes other methods involving demagnetization to zero field, where zero frequency pulses are applied to initiate and monitor evolution. These experiments have been extended to discriminate between different nuclei (e.g., ^{2}D and ^{1}H) in zero field.[12(a)] Finally, this approach introduces the possibility of implementing a number of experiments of value in high field NMR, such as spin echoes,[20] spin decoupling,[21] and multiple pulse NMR,[1,22] to spin systems in zero field. Narrow-band pulsed spin locking of individual transitions in zero field NQR has previously been demonstrated.[23]

C. Relationship to high field methods

In some cases, high field NMR techniques can extract dipolar or quadrupolar couplings from polycrystalline samples. Where dilute heteronuclear spins (e.g., ^{13}C, ^{15}N, or ^{31}P) are present, simple patterns may be obtained by homonuclear dipolar decoupling (which effectively isolates the abundant spins one from another). Only the heteronuclear couplings survive, and spectral simulation may extract these couplings.[24] When combined with magic angle spinning,[25] correlations between the isotropic shifts of heteronuclear spins and the dipole couplings to nearby abundant spins are observed. Couplings smaller than the rotor frequency are eliminated. This information loss is the price paid for the increased resolution with which the largest couplings are measured.

In quadrupolar systems, the powder patterns arise from only local effects, and given adequate signal-to-noise and resolution these single-spin interactions can be reconstructed. Recently a two-dimensional high field NMR technique has been applied to the extraction of quadrupolar couplings where only a portion of the spectrum can be detected.[26] If more than a single type of nucleus contributes to the signal, it may be difficult to separate out the individual contributions. For many spins, and if the entire powder pattern can be observed, the simple form of the quadrupolar (or any other "*inhomogeneous*"[27]) Hamiltonian may allow for "de-Pakeing"[28]; i.e., numerical deconvolution of the spectral patterns into couplings based on an assumed angular dependence and distribution function. If these spectra follow the assumed angular dependence, high resolution, sharp line spectra may result. The zero field NMR and NQR technique we present here may be considered a general experimental approach to de-Pakeing.

D. Outline

In Sec. II a general density operator formalism is presented which provides a simple route to numerical calculation of spectra of disordered systems obtained with sequences like that of Fig. 5. The problem of two identical dipolar coupled spin-1/2 nuclei is solved explicitly. In Sec. III, we treat the more general problem of zero field NMR in dipolar coupled spin systems. Experimental spectra are shown and interpreted. Simulations are given for a number of possible molecular geometries, and the zero field line shapes contrasted with simulated high field powder patterns. We further illustrate the line shapes expected for large numbers of coupled spins. Zero field NMR spectra for heteronuclear spin systems are also discussed. An analytical solution is given for a single I-S pair. This is followed by experimental examples of ^{13}C–^{1}H dipolar zero field spectra. Spectral simulations are presented for these experiments, and also for an I_2S system (appropriate to a $^{13}CH_2$ group).

In Sec. IV, we discuss the application of the technique to zero field NQR studies of integer and half-integer spins. For $I = 1$, $\frac{3}{2}$, and $\frac{5}{2}$ expressions are presented for the observed signal. This is followed by representative experimental high-resolution NQR spectra on powdered samples containing the quadrupolar nuclei ^{2}D, ^{7}Li, and ^{27}Al obtained by the sudden switching technique. Section V considers the effects of molecular motion and sample rotation on zero field spectra. For some simple cases, it is demonstrated how rapid motion is reflected in the spectrum. The combined effects of quadrupolar couplings, motion, and dipolar couplings are analyzed for a deuterated methyl (CD_3) group. Section VI includes a brief description of the experimental approach to high resolution solid state NMR in zero field. This is followed, in Sec. VII, with a presentation of some variations of this sequence, which make use of different initial conditions, different demagnetization conditions, or different detection period sequences. Finally we comment on some further applications, including two-dimensional spectroscopy.[11]

II. BASIC THEORY OF ZERO FIELD NMR

A. Zero field interactions

In this section the interactions referred to in Sec. I as local fields are described more fully by their operator forms. The spin Hamiltonian in zero magnetic field is

$$H = H_D + H_Q + H_J \,. \tag{2}$$

The first term is the direct dipolar Hamiltonian

$$H_D = -\sum_{i<j} \mathbf{I}_i \cdot \mathbf{D}_{ij} \cdot \mathbf{I}_j \,. \tag{3}$$

The second term is the quadrupolar Hamiltonian

$$H_Q = -\sum_k [eQ_i/4\hbar I_i(2I_i - 1)]\,\mathbf{I}_i \cdot \mathbf{V}_i \cdot \mathbf{I}_i \,, \tag{4}$$

where eQ_i is the nuclear quadrupole moment and V_i the electric field gradient tensor of spin i. $H_Q = 0$ for $I_i = 1/2$.

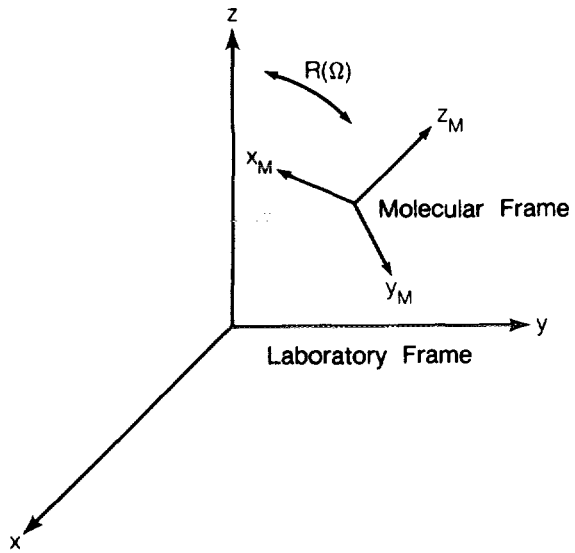

FIG. 7. Relationship between the laboratory frame of reference (xyz) and the molecular frame ($x_M y_M z_M$). The molecular frame is reached by a rotation $R(\Omega)$ about the laboratory-fixed axis system. The most general rotation $R(\Omega)$ is described by the Euler angles and requires rotations about the fixed-frame z, y, and z axes successively. In most NMR applications only the latter two rotations are necessary.

The last term is the indirect, electron mediated spin interaction, or J coupling,

$$H_J = -2\pi \sum_{i<j} \mathbf{I}_i \cdot \mathbf{J}_{ij} \cdot \mathbf{I}_j \,. \tag{5}$$

The J coupling is generally small as compared to the quadrupolar or dipolar couplings in solids. In most systems no substantial error is made in ignoring its effects. It is, of course, the only interaction left in zero field NMR studies of isotropic fluids.[30]

These compact forms for the terms of the zero field Hamiltonian emphasize their invariance, as scalar operators, to simultaneous rotation of space and spin coordinates. For purposes of calculation, a particular coordinate system is chosen and the Hamiltonian expanded as a scalar contraction of spatial factors (spherical harmonic functions) and spin factors (spherical tensor operators). Two such coordinate systems will be used: a lab-based frame, with the z axis in the direction along which a magnetic field may be introduced, and a molecular frame consistently fixed so that an ensemble of identical but arbitrarily oriented spin systems share the same expanded form of the Hamiltonian. The laboratory frame Hamiltonian of Eq. (2) will be called H_L, and the molecular frame form H_M. Operators will be specified as referenced to either the lab or molecular frame with the subscripts L and M. The two frames, and the transformation between them, are shown in Fig. 7.

B. Density operator description

Here we consider the form of the signal for the idealized experiment described above, with instantaneous switching of the applied field, as illustrated in Fig. 5. The time development of the spin degrees of freedom is conveniently described by means of a density operator. The density operator ρ^{Ω} refers to an ensemble of systems with a common orientation Ω of local coordinate systems, and the final signal is then integrated over the orientational distribution in Ω. For the high field part of the experiment, the usual rotating frame interaction picture will be used. Here, we will only be concerned with initial and detected density operators where the rotating frame and the laboratory frame are equivalent and no distinction will be made between the two. This corresponds to stroboscopic observation of the high field signal in multiples of the spectrometer reference frequency which defines the rotating frame.

1. The initial density operator

In the case of a spin system in high magnetic field, the initial density operator $\rho_L(0)$ is given by the usual high field, high-temperature approximation

$$\rho_L(0) = \sum_i \frac{1}{Z_i}(1 + b_i I_{zi}) \tag{6a}$$

and

$$b_i = \frac{\gamma_i \hbar B_0}{kT}, \tag{6b}$$

and the Z_i's represent partition functions for the different spin systems. Since the unit operators [the first terms in the sum of Eq. (6a)] undergo no evolution, we will generally consider only the reduced density operator

$$\rho_L(0) = \sum_i b_i I_{zi} \,. \tag{6c}$$

In homonuclear spin systems, all of the b_i's are identical and without loss of generality, we can choose the proportionality constant b, equal to one. In heteronuclear spin systems, it will prove a notational convenience to both use multiple spin labels (e.g., I and S) and to retain the individual coefficients b_I and b_S.

Most generally, the initial density operator $\rho_L(0)$ may depend parametrically on Ω because the high field Hamiltonian and relaxation rates do. Where the initial condition is high field Zeeman order, however, there is no such initial dependence.

2. Time evolution of the density operator

The time evolution of the density operator is described by the Liouville equation. For time independent Hamiltonians, the integral form of the Liouville equation is

$$\rho(t) = \exp(-iHt)\rho(0)\exp(iHt) \,. \tag{7a}$$

We will always assume that a time dependent Hamiltonian can be separated into n time independent Hamiltonians, where time evolution is given by

$$\rho(t) = \exp(-iH_n t_n)\cdots\exp(-iH_1 t_1)\rho(0)\exp(iH_1 t_1) \cdots \exp(iH_n t_n) \,. \tag{7b}$$

Fourier transformation with respect to any of the t_m yields a normal, one-dimensional spectrum which depends parametrically on all other time variables. Fourier transformation with respect to two different time variables yields a two-dimensional spectrum, which contains not only both indi-

vidual one-dimensional spectra, but also (and more importantly) the correlations between the different time intervals.

3. Transformation between reference frames

The instantaneous change of the Hamiltonian which initiates the evolution period t_1 leaves the system in the same quantum state, i.e., the density operator is unaltered. (This is the sudden approximation of quantum mechanics.) It is more convenient, however, to treat the evolution in a frame where the zero field Hamiltonian is homogeneous; i.e., has the same form for all orientations. This requires that we transform from the lab frame, where the initial density operator was defined, to some consistent molecule-fixed frame via a rotation as shown in Fig. 7. The most general form for the rotation relating two axis systems in space is

$$R(\Omega) = \exp(i\alpha F_z)\exp(i\beta F_y)\exp(i\gamma F_z)\,, \tag{8}$$

where $F = I + J$ is the sum of spin and spatial angular moments in the lab frame, and $\Omega = (\alpha, \beta, \gamma)$ is the set of Euler angles relating the molecular frame to the lab frame. Due to the effective cylindrical symmetry of the high field Hamiltonian, only two of the Euler angles (α and β) are needed. In a powder, R will differ for each orientation of individual crystallites in the externally applied field.

The transformation which relates the density operator in the lab and molecular frame is

$$\rho_M^{\Omega} = R\,\rho_L^{\Omega} R^{-1}\,. \tag{9a}$$

For example, with the density operator of Eq. (6),

$$RI_{zL}R^{-1} = I_{zM}\cos\beta - I_{xM}\sin\beta\cos\alpha + I_{yM}\sin\beta\sin\alpha\,. \tag{9b}$$

Note that the spatial degrees of freedom do not enter since the density operator here describes only the spin system, which for the case of equilibrium in high field is initially independent of orientation. The spin system now evolves under the influence of the zero field Hamiltonians (3)–(5). At a time t_1 the evolved density operator is

$$\rho_M^{\Omega}(t_1) = \exp(-iH_M t_1)\rho_M^{\Omega}(0)\exp(iH_M t_1)\,. \tag{10}$$

Finally, we reexpress the density operator in the lab frame where measurements are made. This is arrived at by inverting the transformation in Eq. (8) and integrating over the distribution $P(\Omega)$ of orientations, i.e.,

$$\rho_L(t_1) = \int R^{-1}\rho_M^{\Omega}(t_1)RP(\Omega)d\Omega \tag{11a}$$

$$= \int R^{-1}\exp(-iH_M t_1)R\rho_L(0)R^{-1} \times \exp(iH_M t_1)RP(\Omega)d\Omega\,. \tag{11b}$$

Equivalently, one might view Eq. (11b) as suggesting a transformation of the evolution operator from a molecular frame to a lab-based frame.

4. Detection of the signal

For the observable, i.e., the operator detected at the end of the zero field evolution period t_1, we take the longitudinal nuclear magnetization. When a large magnetic field $B \gg B_{\rm loc}$ is suddenly reapplied, further evolution of the longitudinal magnetization (and commuting higher rank tensor operators) is terminated. Other observables decay with a time constant $\sim M_2^{-1/2}$ (in solids, ~ 10–$100\,\mu$s) where M_2 is the second moment of the high field spectrum. In practice, longitudinal magnetization is not an observable, and the detection sequences used require the further application of pulsed rf fields in high field. Details of the high field detection period t_2, where the signal is actually observed, are given in Sec. VI B. Formally, it is sufficient to assume that I_{zL} itself is observable. For strong rf pulses, this corresponds to evaluating the signal function at a time $t_2 = 0$, i.e., before any evolution under the high field Hamiltonian can occur. Thus, the initial condition and the detected operator are identical. The response for any system orientation Ω is the autocorrelation function of the initial magnetization

$$S^{\Omega}(t_1) = S^{\Omega}(t_1, t_2 = 0) = \mathrm{Tr}[I_{zL}\rho_L^{\Omega}(t_1)] = \mathrm{Tr}[I_{zL}(0)I_{zL}(t_1)]\,, \tag{12}$$

where

$$X(t_1) \equiv \exp(-iHt_1)X(0)\exp(iHt_1) \tag{13}$$

and the Hamiltonian H is assumed to be expressed in the same reference frame as the operators X. (Evolution under H will most conveniently be described in its eigenbasis, and where explicit representations are required all operators will be presented in that basis set.) A consequence of this form is that the ω_1 spectrum appears with all lines in phase for any system orientation.

We have written Eq. (12) as a trace over lab frame operators. The trace, however, is invariant with respect to basis set. Practically, Eq. (12) is more naturally evaluated in the molecular frame where the Hamiltonian, and therefore the evolution operator, is homogeneous. This is equivalent to inserting Eq. (11) and permuting the transformations R in the trace. The trace is performed over molecule-fixed operators and thereafter integrated over the orientational distribution. In this fashion, we arrive at the signal function S^{Ω} for a specific orientation Ω reexpressed in the molecular frame

$$S^{\Omega}(t_1) = \mathrm{Tr}[RI_{zL}R^{-1}\exp(-iH_M t_1) \times RI_{zL}R^{-1}\exp(iH_M t_1)]\,. \tag{14}$$

Expanding the transformation in the Wigner rotation matrices and spherical tensor operators

$$RI_{zL}R^{-1} = D^1_{00}(\Omega)I_{zM} - D^1_{10}(\Omega)(2)^{-1/2}I_{+M} + D^1_{-10}(\Omega)(2)^{-1/2}I_{-M} \tag{15a}$$

or, again, in the more familiar basis set of the angular momentum operators

$$RI_{zL}R^{-1} = \cos\beta I_{zM} - \sin\beta\cos\alpha I_{xM} + \sin\beta\sin\alpha I_{yM}\,. \tag{15b}$$

Substitution of Eq. (15) into Eq. (14) yields

$$S^{\Omega}(t_1) = \mathrm{Tr}\{[\cos\beta I_{zM}(0) - \sin\beta\cos\alpha I_{xM}(0) + \sin\beta\sin\alpha I_{yM}(0)][\cos\beta I_{zM}(t_1) - \sin\beta\cos\alpha I_{xM}(t_1) + \sin\beta\sin\alpha I_{yM}(t_1)]\}\,. \tag{16}$$

The spectrometer detects only the total signal integrated over the distribution $P(\Omega)$ of system orientations:

$$S(t_1) = \int S^{\Omega}(t_1) P(\Omega) d\Omega \,. \tag{17}$$

For a powder distribution, $P(\Omega) =$ constant. Only products of operators with even powers of $\cos\alpha$ and $\sin\alpha$ survive the integration over α; thus, the integrated signal is

$$\begin{aligned} S(t_1) &= \mathrm{Tr}[(1/3) I_{zM}(0) I_{zM}(t_1) + (1/6) I_{+M}(0) I_{-M}(t_1) \\ &\quad + (1/6) I_{-M}(0) I_{+M}(t_1)] \qquad (18a) \\ &= (1/3)\mathrm{Tr}[I_{xM}(0) I_{xM}(t_1) + I_{yM}(0) I_{yM}(t_1) \\ &\quad + I_{zM}(0) I_{zM}(t_1)] \qquad (18b) \\ &= (1/3) \sum_{i,j} \sum_{p=x,y,z} |\langle i|I_{pM}|j\rangle|^2 \cos\omega_{ji} t \,, \qquad (18c) \end{aligned}$$

where energies are expressed in angular frequency units and

$$\omega_{ji} = (E_j - E_i) = -\omega_{ij} \,. \tag{19}$$

This orthogonality condition is equivalent to stating that the bulk magnetization vector, prepared parallel to the externally applied field, remains linearly polarized along the applied field for all times t_1 if the distribution of Ω is uniform in the azimuthal angle α. For example, in powder samples there is no reason to attempt to design schemes which trap and observe components of the evolved magnetization orthogonal to the initial magnetization. The oscillating magnetization is a real number, and positive and negative frequencies cannot be distinguished.

Equation (18) provides a practical prescription for the calculation of zero field spectra. The zero field Hamiltonian is calculated and diagonalized. Then the angular momentum operators are written in the zero field basis set. Relative intensities correspond to the absolute square of these dipole matrix elements summed over the three components. The frequencies correspond to differences between the energy levels coupled by these operators. Whereas the high field truncated Hamiltonians have eigenvalues which depend on orientation (and thus each sample orientation contributes differently to the observed spectrum) the zero field Hamiltonians (2)–(4) are homogeneous, and the energy levels and thus transition frequencies are identical for all crystallites.

Some theoretical results using this formalism have recently appeared.[31]

C. Zero field NMR of two equivalent spin-1/2 nuclei

In order to make concrete the procedure described above, it can be applied to predicting and interpreting the spectrum of two dipolar coupled homonuclear spin-1/2 nuclei. This situation is closely approximated experimentally by the spin system $Ba(ClO_3)_2 \cdot H_2O$ whose zero field spectrum is shown in Fig. 4. Rather than starting from one of the general forms of Eq. (18), in this section the intermediate steps are made explicit as a pedagogical example.

Assuming that the spin system has been allowed to equilibrate with the lattice, and acquired the bulk magnetization consistent with Curie law

$$\rho(0) = I_{zL} = I_{z1L} + I_{z2L} \,. \tag{20}$$

For two static protons (or where the protons are hopping between sites so as to leave the coupling unaveraged, as in many crystalline hydrates), the dipolar Hamiltonian is most naturally written in a basis set where the z axis is chosen along the internuclear vector, and

$$H = -\omega_D (3 I_{z1M} I_{z2M} - I_1 \cdot I_2) \,, \tag{21}$$

where

$$\omega_D = \frac{\gamma^2 \hbar}{r^3} \,. \tag{22}$$

In Table A1 of Appendix A we summarize the matrix elements of the Hamiltonian and the angular momentum operators I_{xM}, I_{yM}, and I_{zM} in the molecular eigenbasis. Time evolution in Eq. (7) is easily accounted for once we are in the eigenbasis of the Hamiltonian. For individual matrix elements of ρ, and where all energies are expressed in angular frequencies

$$\begin{aligned} \langle a|\rho(t)|b\rangle &= \langle a|\exp(-iHt)\rho(0)\exp(iHt)|b\rangle \\ &= \langle a|\exp-(-iE_a t)\rho(0)\exp(iE_b t)|b\rangle \\ &= \exp(i\omega_{ba} t)\,\langle a|\rho(0)|b\rangle \,. \end{aligned} \tag{23}$$

For the triplet manifold of two identical spin-1/2 nuclei (or a real spin-1 system), and in the basis set of Table A1 of Appendix A,

$$I_{xM}(t_1) = I_{xM}\cos\omega_{23} t_1 + (I_{yM} I_{zM} + I_{zM} I_{yM})\sin\omega_{23} t_1 \,, \tag{24a}$$

$$I_{yM}(t_1) = I_{yM}\cos\omega_{31} t_1 + (I_{xM} I_{zM} + I_{zM} I_{xM})\sin\omega_{31} t_1 \,, \tag{24b}$$

and

$$I_{zM}(t_1) = I_{zM}\cos\omega_{12} t_1 + (I_{xM} I_{yM} + I_{yM} I_{xM})\sin\omega_{12} t_1 \,. \tag{24c}$$

The operators $I_{iM} I_{jM} + I_{jM} I_{iM}$ are orthogonal to the angular momenta I_{kM}. They correspond to higher rank tensor operators T^k_q (with $k > 1$) such that $\mathrm{Tr}(I_i T^k_q) = 0$; thus only terms like $I_i(0) I_i(t_1)$ contribute to the signal function. Therefore,

$$\begin{aligned} &S^{\Omega}(t_1) \\ &= \mathrm{Tr}[I_{zM}(0) I_{zM}(t_1)\cos^2\beta + I_{xM}(0) I_{xM}(t_1)\sin^2\beta\cos^2\alpha \\ &\quad + I_{yM}(0) I_{yM}(t_1)\sin^2\beta\sin^2\alpha] \,. \end{aligned} \tag{25}$$

For the Hamiltonian of Eq. (21),[32]

$$\omega_{12} = 0 \tag{26a}$$

and

$$-\omega_{23} = \omega_{31} = \tfrac{3}{2}\omega_D \,. \tag{26b}$$

Substituting, taking the traces and normalizing the signal function to unity for $t_1 = 0$:

$$\begin{aligned} S^{\Omega}(t_1) &= \cos^2\beta + \sin^2\beta\sin^2\alpha\cos(\tfrac{3}{2}\omega_D t_1) \\ &\quad + \sin^2\beta\cos^2\alpha\cos(\tfrac{3}{2}\omega_D t_1) \,. \end{aligned} \tag{27}$$

Finally, the signal must be integrated over the powder distribution:

$$S(t_1) = \frac{1}{4\pi}\int S^{\Omega}(t_1) d(\cos\beta) d\alpha \tag{28}$$

$$= [\tfrac{1}{3} + \tfrac{2}{3}\cos(\tfrac{3}{2}\omega_D t_1)] \,. \tag{29}$$

The Fourier transform of this signal function consists of three equally spaced lines of equal intensity, and closely approximates the spectrum of Fig. 4. In addition to the features

predicted by the above treatment, the spectrum shows additional, smaller features at twice the predicted frequency. These are presumably due to the interactions of one crystalline water molecule with its neighbors. The measured value of ω_D corresponds to a proton–proton distance of 1.62 ± 0.01Å.

A more detailed treatment of the case of two equivalent spin-1/2 nuclei is given in Appendix A.

III. ZERO FIELD NMR OF DIPOLAR COUPLED SPIN-1/2 NUCLEI

A. General dipolar coupled spin systems

Where the dipole–dipole Hamiltonian for N spins,

$$H_D = \sum_{i<j}^{N} \frac{\gamma_i \gamma_j \hbar}{r_{ij}^3} \left[\mathbf{I}_i \cdot \mathbf{I}_j - \frac{3}{r_{ij}^2} (\mathbf{I}_i \cdot \mathbf{r}_{ij})(\mathbf{I}_j \cdot \mathbf{r}_{ij}) \right] \tag{30}$$

dominates the spectral features, both the high field and zero field spectra are likely to be quite complicated. Fundamentally, the problem arises because the spectrum is characteristic of groupings of spins and their relative spin orientations. In contrast to the two-spin case discussed previously, there is no choice of axis system which makes Eq. (30) take on any simple form. As the number of strongly interacting spins N becomes large, the number of combinations of spin orientations (and thus energy levels) increases rapidly (as 2^N). While only a small number of couplings serve to completely characterize the geometry [there are only $N(N-1)/2$ distinct couplings], these couplings may result in an enormous number of line frequencies. A similar problem is confronted in the analyses of small molecules ordered in liquid crystalline phases, where special techniques are required to resolve sufficient numbers of lines to make sense of large (>6) groupings of spins.[33] The familiar angular momentum selection rule

$$n = \Delta m = \pm 1 \tag{31}$$

is not applicable in the absence of an applied field, as no unique axis exists (except in special cases) along which the nuclear spin angular momentum is quantized.

As described in Sec. II C, the zero field spectrum is calculated by looking at matrix elements of I_{xM}, I_{yM}, and I_{zM}. Generally, all energy levels will be connected to all others by these selection rules; i.e., matrix elements of I_{xM}, I_{yM}, or I_{zM} will be nonzero for all pairs of eigenstates. In the absence of symmetry constraints, one expects the zero field spectrum to consist of a maximum of W lines, where

$$W = 2^N(2^N - 1), \tag{32}$$

i.e., a pair of lines appears centered around zero frequency for each pair of energy levels. Fortunately, this estimate severely overcounts the number of lines expected for N an odd number. From Kramer's theorem, and as a consequence of time reversal symmetry, for N odd, all eigenstates of the zero field Hamiltonian are at least doubly degenerate. Therefore, the maximum number of transition frequencies is greatly reduced; and

$$\begin{aligned} W &= 2^N(2^N - 1), \quad N = 2, 4, 6, \ldots, \\ W &= 2^{N-1}(2^{N-1} - 1) + 1, \quad N = 3, 5, 7, \ldots . \end{aligned} \tag{33}$$

The extra line which appears for N odd is at zero frequency and represents matrix elements which couple degenerate states. For small N, symmetry considerations may markedly reduce the actual number of lines observed. In particular, in the homonuclear two-spin case we have shown that only 3 of the predicted maximum of 12 lines are observed.

B. Homonuclear spin systems

1. Structure determination: Four coupled ^{1}H nuclei

For $N = 4$, Eq. (33) predicts the possibility that 240 discrete lines might be observed in the zero field spectrum. Unfortunately, not all of these lines can be resolved in most cases. In Sec. I, we compared single crystal and zero field NMR spectra. The linewidths of individual lines in these spectra are comparable, and still ~ 1 kHz wide or greater. These linewidths generally arise from two types of effects: lifetime broadening due to finite T_1's, or more usually the small couplings to neighboring spins which fail to split lines. Much can be learned from the conceptually simple method of choosing a likely geometry, calculating a spectrum, broadening it to match the observed linewidths and shapes, and modifying the geometry on the basis of the match to the observed spectrum. As an example of the detailed information which zero field NMR can provide, Fig. 8 shows the zero field spectrum of the four proton system, 1,2,3,4-tetrachloronaphthalene bis (hexachlorocyclopentadiene) ad-

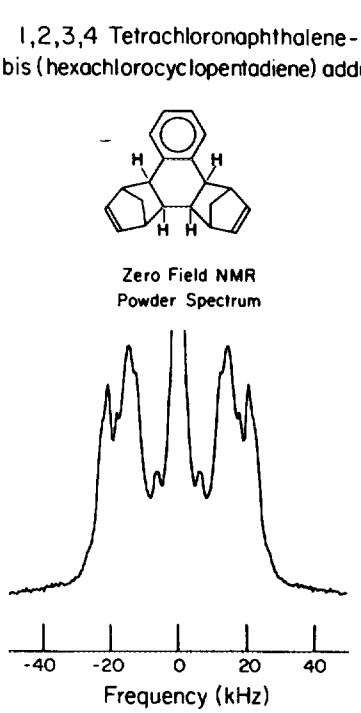

FIG. 8. Top: the molecule 1,2,3,4-tetrachloronaphthalene bis(hexachlorocyclopentadiene) adduct. The configuration of the four ^{1}H atoms about the central ring is unknown. All other ring substituents are perchlorinated. The high field spectrum of this compound is shown in Fig. 3. Bottom: zero field NMR spectrum. The sharp peak at zero frequency is truncated for purposes of display. The evolved zero field magnetization is sampled at 5 μs increments giving an effective zero field bandwidth of $\pm$ 100 kHz. Only half that spectral width is plotted.

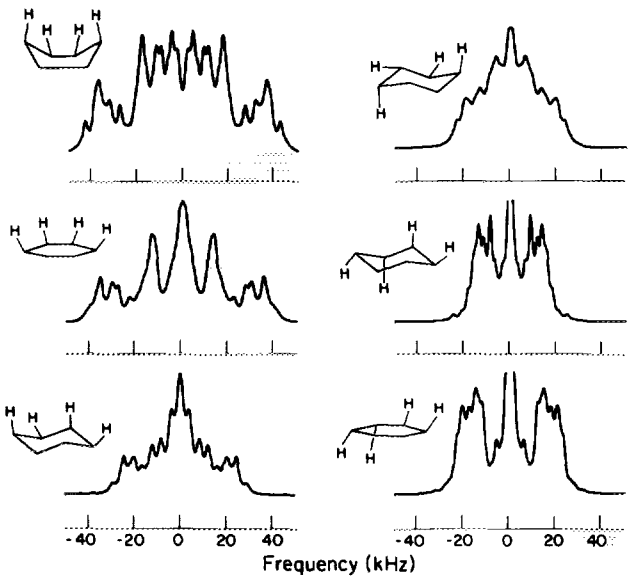

FIG. 9. Simulated zero field spectra for six possible configurations of the ^{1}H nuclei about the central ring in 1,2,3,4-tetrachloronaphthalene bix(hexachlorocyclopentadiene) adduct. For clarity, only the configuration of the central ring is shown, at left of the associated spectrum. For each configuration, the zero field spectrum is calculated, broadened to fit the observed linewidths, and plotted. The simulation at bottom right closely resembles the observed spectrum (Fig. 8). A C_2 axis of symmetry, which interconverts the two innermost (1 and 1') and two outermost (2 and 2') sites is assumed. Because of the assumed symmetry, only four distances characterize the simulation: $r_{11'} = 2.83$ Å, $r_{12} = 2.22$ Å, $r_{12'} = 4.34$ Å, and $r_{22'} = 5.01$ Å.

duct, whose high field spectrum was shown in Fig. 4. In Fig. 9 we have calculated the spectra expected for a number of different possible geometries. By comparing the observed pattern (Fig. 8, bottom) to computer simulations, most possibilities are readily excluded. The geometry most consistent with the experimental zero field spectrum is clearly that at the bottom right in Fig. 9. Minor changes in geometry (a change of no more than 0.05 Å) could be readily observed even in powder samples. Another example of the sensitivity of zero field NMR to small structural perturbations for isolated spin systems will be published elsewhere.[34]

2. Simulations for representative spin systems

In Fig. 10, we compare calculated zero field and high field spectra for a number of representative distributions of ^{1}H nuclear spins. Comparison of calculated high field powder patterns and zero field spectra illustrates the increase in resolution expected by the zero field technique. All simulations assume the axially symmetric, static dipole–dipole coupling of Eq. (30) and an empirically applied broadening function. The high field powder spectra were calculated as a sum over a finite number of orientations. This sum is then convoluted with a Gaussian broadening function to account for the effects of orientations not actually sampled and residual couplings. The zero field powder spectra are solved exactly using the method of Sec. II B 4 (although generally, a solution

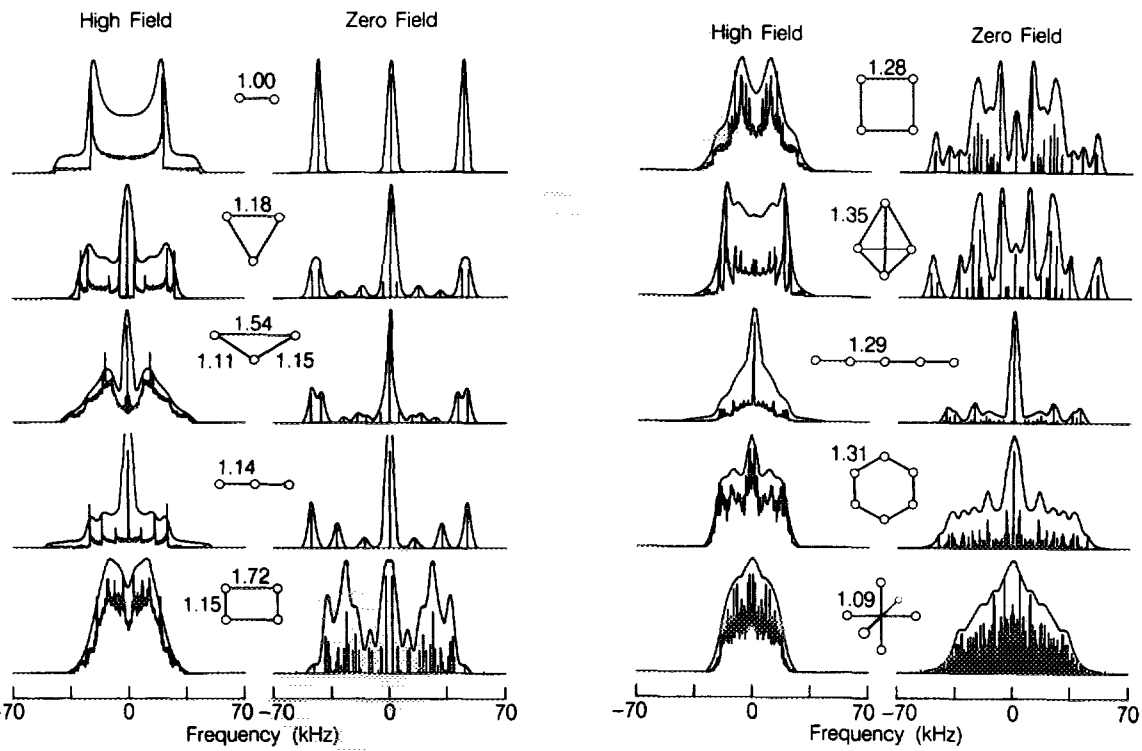

FIG. 10. Calculated high field and zero field NMR spectra for small N systems of coupled, static, and equivalent ^{1}H nuclei with various geometries. Distances were chosen so that all the spectra appear to fit in the same frequency range. The base distance is that of the two-spin Pake pattern where $r_{ij} = 1.60$ Å gives a spectrum whose frequency spread is that of the scale at bottom. Each of the high field spectra is calculated by summing the simulated spectra for a large number of different orientations of the spin system relative to an externally applied laboratory magnetic field (varying from 14 400 orientations for the three-spin systems to 400 for the six-spin systems). The resulting spectra (the insets) are then convoluted with a Gaussian line shape. The zero field spectra are calculated by the procedure indicated in Sec. II B 4. The delta function simulations (the insets) are convoluted with the same Gaussian broadening function. In most of the odd-spin systems simulations, a sharp zero frequency peak has been truncated in the unbroadened spectra. Occasionally the broadened spectrum is also truncated (where indicated by broken lines).

for the eigenvalues of H_M requires numerical techniques). These spectra are broadened with the same Gaussian line shape, although a Lorentzian broadening function seems to more accurately reproduce experimental results than does the Gaussian line shape normally assumed in high field NMR.

3. Zero field NMR for large N

The problem of spin absorption in zero applied field has been addressed by a number of authors.[7,14,35] Most of this work has concentrated on spectral line shapes for quadrupolar systems, with possible modifications for the effects of dipolar couplings or motion. Because experimental results for systems of dipolar coupled systems in zero field are rare, this problem has received much less attention. For systems of many coupled spins, the absorption band tends toward a characteristic shape with long broad tails and a narrow, low-frequency component. This behavior was first predicted by Kubo and Toyabe,[36] and has, until now, found experimental verification primarily in the study of the decay of muon polarization.[37] In the limit of no relaxation and static dipolar fields, the Kubo–Toyabe statistical theory predicts

$$S(t_1) = \tfrac{1}{3} + \tfrac{2}{3}(1 - \Delta^2 t_1^2)\exp(-\Delta^2 t_1^2/2)\,, \tag{34}$$

where Δ represents the distribution of local fields, and in some suitably chosen local reference frame

$$\langle H_x^2 \rangle = \langle H_y^2 \rangle = \langle H_z^2 \rangle = \Delta^2/\gamma^2\,. \tag{35}$$

Roughly speaking, this corresponds to a spectrum with a sharp component at zero frequency, and a broad non-Gaussian line shape extending to higher frequencies. Relaxation serves mainly to broaden out the δ function at zero frequency into a near-Lorentzian line. This type of line shape is frequently observed in our zero field experiment on dense systems of spin-1/2 nuclei. Figure 11 shows one example, the zero field spectrum of polycrystalline squaric acid.[38]

4. Effects of isotopic dilution in zero field

Frequently, it is possible to achieve the required isolation of small, ^1H-containing spin systems by isotopic dilution, e.g., by replacing some large percentage of the molecules with their perdeuterated analogs. The advantage of this is twofold: First, the γ of the deuteron ~ 0.15 that of the proton, thus reducing the coupling to spins outside the system of interest. Additionally, the deuteron is a spin-1 nucleus and possesses a quadrupole moment. If the local electric field gradient is not axially symmetric, then the dipolar coupling between integer and half-integer spins is quenched in zero field.[35(f),35(g)] We have previously used this technique to advantage in acquiring the zero field NMR spectrum of polycrystalline dimethylterephthalate.[5] An example of the increased resolution possible, and of the transition between the statistical, many-body behavior to isolated spin, sharp line limits is shown in Fig. 12, where we present zero field spectra of sodium acetate trihydrate-d_6 ($NaOAc{\cdot}3D_2O$) as a function of increasing dilution. Resolution increases as we replace CH_3 groups with CD_3 groups. The observed spectrum of this methyl group corresponds to rapid rotation of the CH_3 group about its symmetry axis,[39] and will be more completely described in Sec. V A.

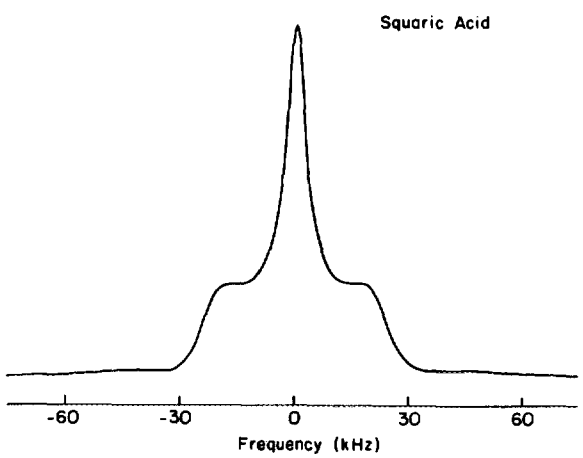

FIG. 11. Zero field ^1H NMR spectrum of polycrystalline squaric acid. The flat wings and sharp central peak are of the form predicted by the Kubo–Toyabe theory [i.e., the Fourier transform of Eq. (34)].

C. Heteronuclear spin-1/2 systems

Commonly, spin systems of interest contain a heteronuclear (S) spin (such as ^{13}C, ^{31}P, or ^{15}N) in addition to protons. Because of the difficulties described in Secs. III B 2–III B 4 of the previous section, most high field dipolar studies exploit the natural isolation of these "rare" spins to make high field dipolar spectra tractable.[24,25] In this section, we consider some of the differences between zero field NMR spectra of homonuclear spins systems, described above, and heteronuclear systems where two different Zeeman spin reservoirs can be identified in high field.

As a consequence of the differing magnetogyric ratios γ_I and γ_S, the initial spin density operator [Eq. (6)] can have

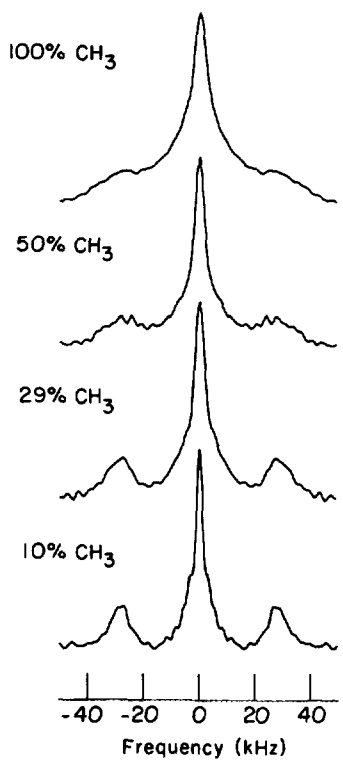

FIG. 12. Zero field NMR spectra of polycrystalline CH_3 group in sodium acetate ($NaOAc{\cdot}3D_2O$), as a function of increasing replacement of CH_3 groups by CD_3 groups. At top, the spectrum of the system with 100% CH_3 groups. Intermolecular couplings are strong, so little local structure can be resolved. Instead, the spectrum is similar to that of Fig. 11. As large numbers of CH_3 groups are replaced by CD_3 groups, the spectrum becomes increasingly well resolved, and sharp features characteristic of the individual methyl groups appear. Assuming rapid rotation exclusively about the C_3 axis, and that the observed splitting in the most dilute case is due only to the intramethyl group couplings, $\langle r^{-3} \rangle^{-1/3} = 1.89$ Å.

different coefficients b_I and b_S for each nuclear spin type. The net alignment of each spin species in the applied magnetic field is proportional to its magnetogyric ratio, and I_z and S_z are separate constants of the motion. Making explicit what distinguishes the heteronuclear case from the homonuclear case, we can write the initial condition prepared in high field as

$$\rho = b_I I_z + b_S S_z, \tag{36}$$

where b_I and b_S represent, respectively, the initial prepared polarizations for each spin system, and the operators I_z and S_z imply a summation over all similar nuclei. For later convenience, we rewrite this as

$$\rho = (b_I + b_S)(I_z + S_z)/2 + (b_I - b_S)(I_z - S_z)/2. \tag{37}$$

First we calculate the spectrum for a single I spin coupled to one S spin. Given the heteronuclear dipolar Hamiltonian,

$$H_D = -\frac{\gamma_I \gamma_S \hbar}{r^3}(3I_z S_z - I \cdot S), \tag{38}$$

we proceed precisely as above in the homonuclear case. The heteronuclear Hamiltonian (38) is identical to Eq. (21) except that we have labeled the spins I and S instead of 1 and 2, and their γ's are no longer equal; therefore, the energy level structure of the heteronuclear pair is identical (to within a scaling constant) to that of the homonuclear pair. The initial density matrix, however, is different. As before, we transform via R into the molecular frame. The first, symmetric term in Eq. (37), which corresponds to the average polarization shared by the two spins in high field, gives rise to precisely those spectral features observed in the homonuclear case, i.e., transitions within the triplet manifold. The second, antisymmetric term, which corresponds to the difference in initial polarizations, produces lines at new frequencies corresponding to transitions between the singlet and triplet manifolds.

An exact calculation proceeds generally as detailed for the homonuclear two spin-1/2 case solved in Sec. II C. Similar transformations relate the high field and local frames. But the difference in high field affects not only the initially prepared operator $\rho_L(0)$. The operator detected in high field is I_{zL} or S_{zL} alone. Thus the signal is given by

$$S^{\Omega}(t_1) = \mathrm{Tr}[I_{zL}\, \rho_L^{\Omega}(t_1)] \tag{39}$$

if the zero field evolution is observed via its effect on the I spin magnetization, or by

$$S^{\Omega}(t_1) = \mathrm{Tr}[S_{zL}\, \rho_L^{\Omega}(t_1)] \tag{40}$$

if the S spins are observed. For a single I spin interacting with one S spin the zero field free induction decay[30] is

$$M_z(t_1) = \tfrac{1}{3}\{\tfrac{1}{2}(b_I + b_S) + (b_I + b_S)\cos(\tfrac{3}{2}\omega_D t_1) \pm [(b_I - b_S)\cos(\tfrac{1}{2}\omega_D t_1) + \tfrac{1}{2}(b_I - b_S)\cos(\omega_D t_1)]\}, \tag{41}$$

where the $+$ sign holds when the I nuclei are detected, and the $-$ sign when the S nuclei are detected.

Since b_I and b_S may be separately controlled in high field, it is possible to manipulate the initial condition so as to change the observed spectrum. One simple possibility is to bring the two spin species into a state of equal initial polarizations. This can readily be accomplished by partially presaturating the high γ nucleus with a suitably chosen rf pulse in high field, or by prepolarizing the low γ nuclei with various high or zero field mixing techniques. One possibility is to adiabatically cycle to zero field, followed by remagnetization prior to initiating the field cycle described above. Polarization is irreversibly transferred from the more ordered spin system by spin mixing where the local fields are larger than the applied fields.[40] Alternatively, one might use normal high field pulsed or cw rf techniques to adjust the initial density operator $\rho(0)$ so as to simplify the resulting spectra.[30,41,42] An illustration of the different spectra which may arise from the different initial conditions possible in ^{13}C-enriched β-calcium formate [$Ca(HCOO)_2$] is shown in Fig. 13. When the initial condition is $I_z + S_z$ the system behaves like a homonuclear spin system and when it is like $I_z - S_z$ the homonuclear lines disappear.

Energy levels and allowed transition frequencies for the two types of two-spin systems are summarized in Fig. 14. We note that in the heteronuclear two spin case, several of the lines predicted in Eq. (33) but missing in the homonuclear case appear. The remainder of these missing lines become allowed only when we include the possible effects of motional averaging, which may split the energies of the two degenerate eigenstates in the triplet manifold of the dipolar Hamiltonian.

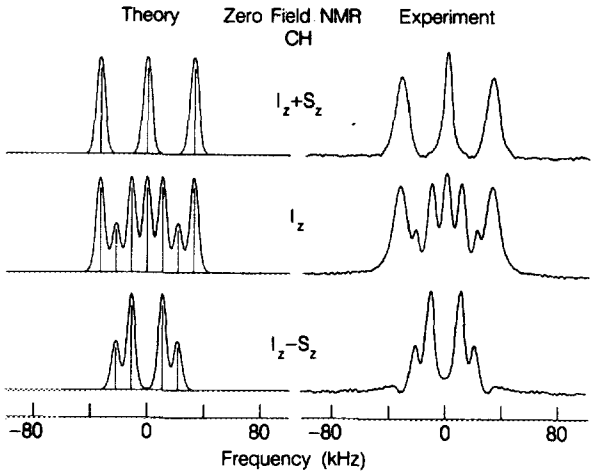

FIG. 13. Left: theoretical zero field NMR spectra of a ^{13}C–^{1}H dipolar coupled pair; $r_{C\text{-}H} = 1.095$ Å. Spectra are shown as a function of relative initial polarizations of the two nuclei. The stick spectra are the prediction of Eq. (41). Superposed are the spectra convoluted with a Lorentzian line 6 kHz wide at half-maximum. Right: experimental spectra of the ^{13}C–^{1}H pair in 90% ^{13}C β-calcium formate [$Ca(HCOO)_2$]. Top and bottom: the ^{13}C nuclei are prepolarized to ~ 1.6 times their equilibrium polarization by a zero field cycle where evolution is allowed to take place for 32 μs. The sample is returned to high field, where a strong rf pulse at the ^{1}H Larmor frequency (185 MHz) is applied. At top, a 66° pulse destroys 60% of the initial ^{1}H magnetization and equalizes the initial spin ordering of the two spin species. At bottom, a 114° pulse destroys the same 60% of the initial ^{1}H magnetization and inverts the rest. In the center, both spin systems are depolarized in zero field, and the sample returned to high field for a time long compared to T_{1H} ($\sim$10 s) and short compared to T_{1C} ($\sim$ several minutes). In high field, the ^{1}H magnetization is observed. The observed dipolar coupling corresponds to $\langle r^{-3}\rangle^{-1/3} = 1.11$ Å.

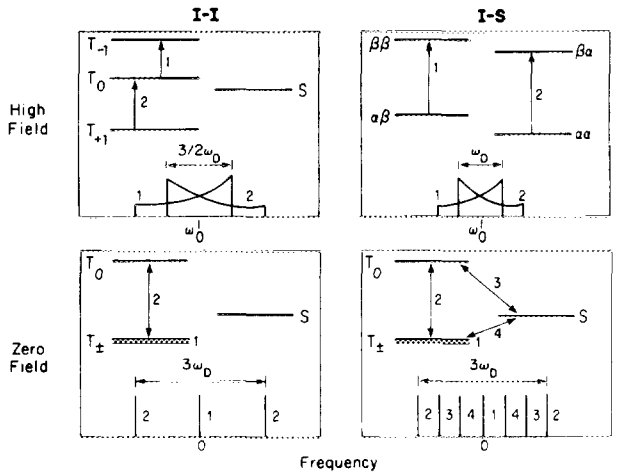

FIG. 14. Summary of the high field and zero field Hamiltonians, eigenstates, and spectra for homonuclear (I–I) and heteronuclear (I–S) dipole coupled pairs. Transitions are indicated by the arrows. In high field, the transition energies are orientation dependent and the spectrum is a continuous absorption band. The zero field energy levels are orientation independent, and the zero field spectrum consists of a finite number of absorption lines. In the homonuclear case, only transitions within the triplet manifold are allowed (both in high and zero field).

Similar effects are expected to occur for the more complicated interactions between more than two spin-1/2 nuclei. Simulations for the specific case of a $^{13}CH_2$ group are shown in Fig. 15. For the initial condition $b_I = b_S$, the simplest spectrum results. We defer until we treat motional averaging the simulation of $^{13}CH_3$.

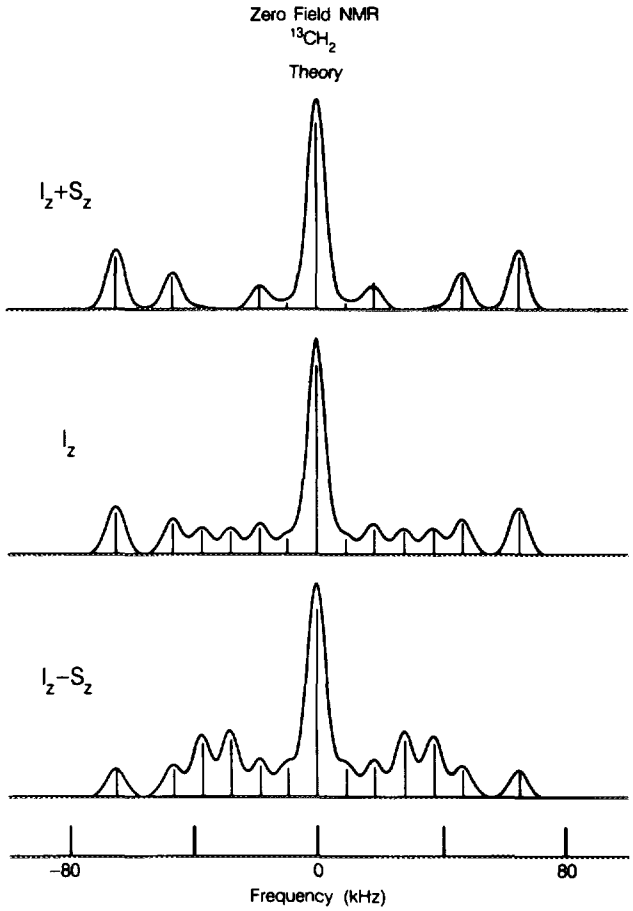

FIG. 15. Simulated zero field spectra of $^{13}CH_2$ groups, as a function of initial condition prepared in high field and with high field detection of the ^1H nuclei. The assumed geometry is $r_{C\text{-}H1} = r_{C\text{-}H2} = 1.095$ Å and a tetrahedral bond angle. The stick spectra are indicated as insets with, superposed, 6 kHz FWHM Lorentzian broadened lines.

IV. TIME DOMAIN NQR OF QUADRUPOLAR NUCLEI

A. Overview

The interactions of the local electric field gradients with the quadrupole moments of nuclei with $I>1$ often give a more detailed description of the local environment than do chemical shifts, but are less frequently measured. Like a chemical shift, but in contrast to a dipolar coupling, the quadrupole interaction is a single nucleus property, and leads to spectra where lines are readily associated with a particular site. A convenient representation of the quadrupole Hamiltonian, Eq. (3), is in the molecular frame where the field gradient tensor is diagonal[14]

$$H_{QM} = -A\,[3I_{zM}^2 - I(I+1) + \eta(I_{xM}^2 - I_{yM}^2)], \tag{42a}$$

where

$$A = \frac{e^2qQ}{4\hbar I(2I-1)}, \tag{42b}$$

$$eq = V_{zz}, \tag{42c}$$

and

$$\eta = \frac{V_{xx} - V_{yy}}{V_{zz}}. \tag{42d}$$

Conventionally,

$$|V_{zz}| > |V_{yy}| > |V_{xx}|. \tag{42e}$$

When this interaction dominates, resolution decreases only linearly with the number of different types of sites. Multiplet structure, due to dipolar coupling, is often a small pertrubation and may provide additional information on the relative proximity of sites without seriously compromising interpertability. This is similar to the situation of chemical shifts and scalar couplings in liquids.

Previous methods for obtaining such NQR spectra in zero field were reviewed briefly in the Introduction. (The NMR dipolar spectra are displayed with both positive and negative frequencies, whereas the quadrupolar spectra are shown with only positive frequencies.) The present form of the time domain zero field experiment (Fig. 5) is most valuable for systems with quadrupole frequencies of less than about 1 MHz. It is for these low frequency systems that other approaches are most difficult.

NQR spectra of integer and half-integer spins differ greatly. A more complete presentation of the quantum mechanics of quadrupolar spin systems is given in the standard NQR references.[14] Here we will briefly review the important points which have a bearing on the interpretation of our experimental spectra.

B. Spin $I = 1$ (^2D and ^{14}N)

Formally, the Hamiltonian of an isolated spin-1 nucleus closely resembles the dipolar Hamiltonian for two spin-1/2

nuclei, and the three energy levels of the spin-1 nucleus are similar to the triplet manifold of the dipolar-coupled pair. The main difference is that the static field gradient tensor V is rarely axially symmetric, while it is only through the effects of motion that the dipolar tensor may become asymmetric. An isolated spin-1 nucleus typically has three nondegenerate energy levels and thus the possibility of three different resonance frequencies. The evaluation of Eq. (18) precisely parallels the treatment of Sec. II C for the triplet manifold of two homonuclear spin-1/2 particles. The only difference is in the eigenvalues of the Hamiltonian. For the general case of a single deuteron with nonvanishing asymmetry parameter η, the energies of the transitions are

$$\omega_{31} = (3 - \eta)A,$$
$$\omega_{23} = -(3 + \eta)A, \tag{43}$$
$$\omega_{12} = 2\eta A.$$

Substituting these values into Eqs. (24) and (25) gives the zero field time domain signal[43]

$$S(t_1) = \tfrac{1}{3}[\cos 2\eta A t_1 + \cos(3 - \eta)A t_1 + \cos(3 + \eta)A t_1], \tag{44}$$

where, for $I = 1$, $A = e^2qQ/4\hbar$. This interferogram reduces to that of Eq. (29) when $\eta = 0$ and we substitute the appropriate quadrupolar frequency. Each isolated deuteron site contributes three lines of equal intensity. As η is typically small, one line appears at a very low frequency and is rarely observed by cw methods.[18] The other two appear as a pair split by the frequency of the low frequency line. The energy level scheme, and a comparison to the spectra of two-spin dipolar systems, is depicted in Fig. 16. If at least two of the lines can be assigned to a given site the field gradient parameters A and η are determined. Observation of the low frequency lines is important when the sample contains multiple sites as it allows the high frequency transitions to be grouped into pairs for each site. When resolved couplings exist between sites with similar quadrupole tensors, the spectral pattern will require a detailed, and presumably iterative, simulation. Such dipolar structure in spin-1 NQR has previously been observed and explained for N_2, $-ND_2$, and D_2O groups.[44]

The deuterium spectrum of perdeuterated dimethylterephthalate in Fig. 17 illustrates these points. The intense band at 38 kHz is assigned to the methyl groups. As is well known,[45] motional averaging caused by the rapid rotation of the CD_3 group about its C_3 axis accounts for the observed reduction in frequency from the 100–150 kHz range typical of static C–D bonds. No lines are obseved near zero frequency, and therefore $\eta \cong 0$. The high frequency region of Fig. 17 shows four resolved transitions, indicating that there are two distinct aromatic ring sites, corresponding to those near to and far from the methyl groups. Due to low intensity and small splitting of these lines as compared to the broadened zero frequency contribution of the methyl group, no ν_0 lines are resolved.

The spectrum of 1,4-dimethoxybenzene (Fig. 18) shows well resolved lines appearing at all three predicted regions of the spectrum. The ν_0 lines appear at precisely the difference frequencies between pairs of lines at high ($\sim$135 kHz) frequencies. Relative intensities are less distorted than in dimethylterephthalate with similar experimental parameters. Nonetheless, the CD_3 group still appears with greater integrated intensity than do the ring sites. The analysis of the aromatic ring spectrum[43] is straightforward since the four high frequency lines can be sorted into a pair for each type of ring site by using the low frequency ν_0 lines. For the methyl group, both the appearance of low frequency lines which cannot be attributed to ring sites and the number of resolved

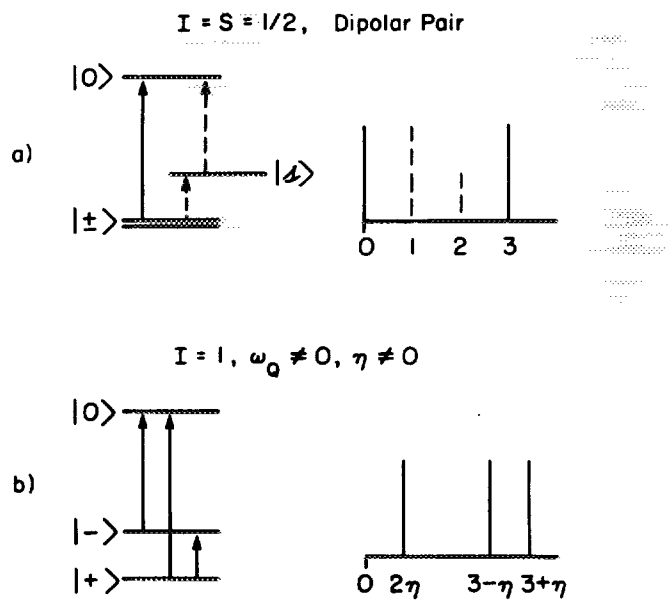

FIG. 16. Comparison of the spectra and Hamiltonians for two dipole-coupled spin-1/2 nuclei, and for a spin-1 quadrupolar system. (a) Summary of the zero field eigenstates and transition energies shown previously in Fig. 14. In keeping with the normal convention of pure NQR, only positive frequencies are shown. Transition frequencies allowed in both homonuclear and heteronuclear spin systems are shown in heavy lines; transitions unique to heteronuclear spin systems are shown with dotted lines. (b) Eigenstates and energy levels for spin-1 system. In the principle axis system of the quadrupolar Hamiltonian, $|+\rangle = 2^{-1/2}(|+1\rangle + |-1\rangle)$, $|-\rangle = -i2^{-1/2}(|+1\rangle - |-1\rangle)$, $|0\rangle = |0\rangle$. The existence of a finite η splits the degeneracy of the $|+\rangle$ and $|-\rangle$ eigenstates. For $\eta = 0$, the spectrum is identical to that of an I–I dipolar coupled pair.

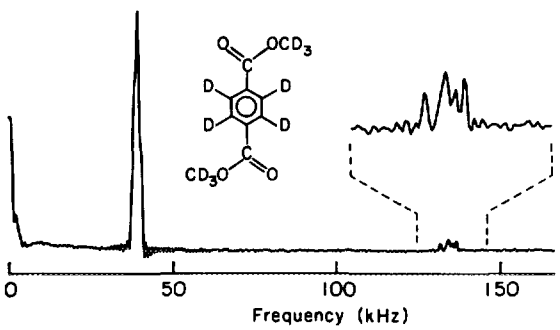

FIG. 17. Zero field ^2D NQR spectrum of perdeuterated polycrystalline 1,4-dimethylterephthalate. The zero field signal was acquired at 3 μs intervals for a total of 1 ms. The high field polarization period was 2 min. The methyl group (CD_3) T_1 is $\sim$10 s; for the ring sites $T_1 > 10$ min. Four lines are observed at frequencies characteristic of the ring sites ($\sim$ 135 kHz). These correspond to a pair of lines for each site, inequivalent because the molecule is locked in the *trans* position in the solid state.

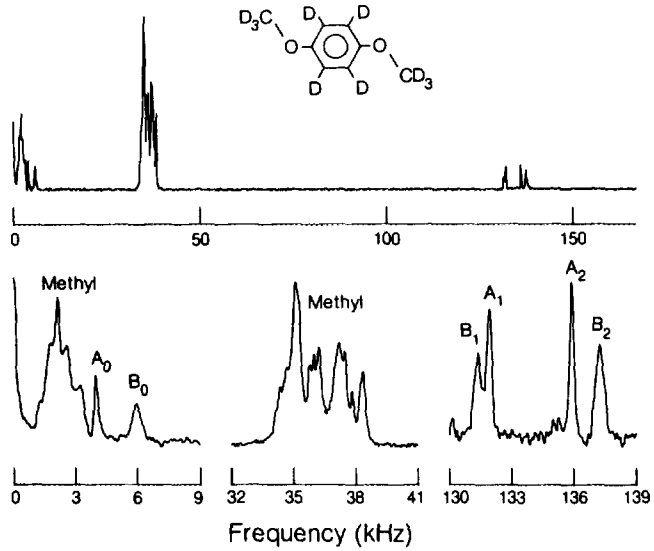

FIG. 18. Zero field ^{2}D NQR spectrum of polycrystalline perdeuterated 1,4-dimethoxybenzene. Top: Fourier transform of the zero field signal (see Fig. 6). Bottom: Expanded views of the three interesting regions of the spectrum. At low frequency (0–9 kHz), the ν_0 lines; ~35–40 kHz, the CD_3 group; and ~131–138 kHz, the ring sites. Four ring site lines are observed, because the positions "near to" and "far from" the methyl groups are distinguishable. In the ν_0 region, the line marked A_0 appears at exactly the difference frequency between the lines A_1 and A_2. Similarly, the triplet of lines B_0, B_1, and B_2, and $e^2qQ/h_A = 178.5$ kHz, $\eta_A = 0.045$; $e^2qQ/h_B = 179.1$ kHz, $\eta_B = 0.067$. The methyl pattern has contributions both from a nonzero value of η and from dipole–dipole couplings within the methyl group.

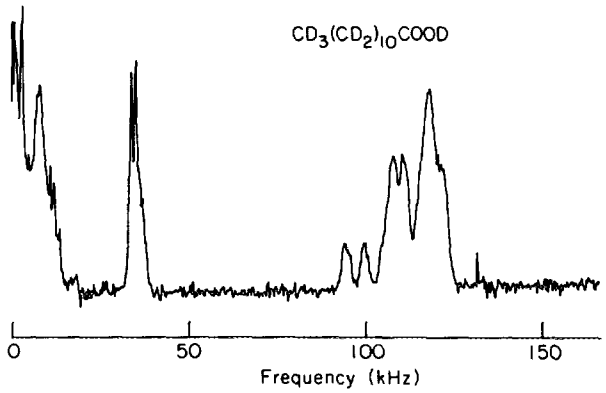

FIG. 19. Zero field ^{2}D NQR spectrum of polycrystalline perdeuterated lauric acid $[CD_3(CD_2)_{10}COOD]$. The spectrum can be divided into three distinct regions: low frequency ν_0 lines, the methyl group region, and the alkane and acid site regions. The high frequency band is broad and reflects the wide range of quadrupolar frequencies along the chain.

peaks apparent in the band of frequencies between 33 and 40 kHz indicate that η is nonnegligible. Despite the rapid rotation of the methyl group, an asymmetry in the local environment leads to an asymmetric, motionally averaged quadrupolar tensor.[45] In addition, the large number of lines cannot be explained without including the effects of the dipolar couplings between deuterons on the methyl group (and possibly to the ring as well). A complete simulation of the observed pattern is not yet available, but values for the motionally averaged quadrupolar tensor alone can be derived using the results of Vega.[35(g)] Dipolar couplings between spin-1 nuclei leave the first moment of the resonance line unshifted. From the measured centers of gravity of the (ν_+,ν_-) and ν_0 regions we find

$$\frac{e^2qQ}{h} = 47.9 \text{ kHz} \tag{45a}$$

and

$$\eta = 0.096. \tag{45b}$$

Spectra of other perdeuterated systems indicate that the zero field spectrometer[46] is capable of exciting and detecting higher frequency zero field coherences. In Fig. 19 we show the zero field spectrum of polycrystalline perdeuterated lauric acid $[CD_3(CD_2)_{10}COOD]$. All regions of the spectrum appear with approximately correct intensities. Unlike other deuterated systems, this long chain molecule shows a broad range of absorption frequencies and few resolved spectral features. It is likely that a distribution of small amplitude librational motions, as discussed in Sec. V C, accounts for this range of quadrupole couplings. Any inhomogeneity in local environment or motion is expected to result in a correspondingly broad range of quadrupolar absorption frequencies.

The predominant contribution to the anomalous intensities often observed in ^{2}D zero field spectra appears to be the differing relaxation rates which characterize the return to equilibrium of the high field magnetization. Because the dipole couplings between deuterons are weak compared to the quadrupolar splittings, chemically different deuterons may have very different T_1's in a solid.[47] Deuterons with short T_1's attain their full equilibrium polarization more rapidly in high field, and thus may begin the field cycle more polarized. Some of this initial advantage may be lost due to more rapid relaxation during the transit to and from zero field. The problem of variable (and often quite long) quadrupolar T_1's is one of the prime motivations for the development of indirect methods of detection, using either frequency domain[9,10] or time domain[12(a)] methods.

C. Half-integral quadrupolar nuclei

We begin with a brief review of some basic results which will prove useful in a discussion of the results obtained in pulsed zero field experiments. From Kramer's theorem[10(b),14,48] each energy level of the zero field Hamiltonian of a half-integer spin is doubly degenerate. Each isolated quadrupolar nucleus in zero field has $2I + 1$ eigenstates; but for half-integral I there are only $(2I + 1)/2$ distinct energy levels. If each energy level is coupled to all others, the predicted number of lines with nonzero frequency is $(4I^2 - 1)/8$. Generally, fewer lines are observed. This is because in the basis set where I_{zM}, the component of the angular momentum along the principal axis of the quadrupolar tensor, is diagonal, the asymmetry parameter η couples only nondegenerate states and, to lowest order, does not perturb the eigenstates. At small values of η, eigenstates may be identified as being almost eigenstates of I_{zM}. Were I_{zM} a good quantum number, the selection rule

$$n_M = \pm 1 \tag{46}$$

would hold, and only I-1/2 distinct nonzero frequencies

would be observed for each half-integral spin I. Even where an asymmetry parameter breaks this selection rule, the amplitudes of the "forbidden" lines are typically small.

The high field powder spectrum for half-integral spins consists of a prominent central peak due to the ($|1/2\rangle \rightarrow |-1/2\rangle$) transition and weak and broad satellites. The latter are spread over a wide frequency range by the distribution of first order quadrupole energies, and are therefore rarely distinguished from the base line. In Appendix B we consider the case where the detection bandwidth in t_2 is such that only the central transition contributes appreciably to the signal. In such a case, the relative line amplitudes in zero field are preserved (as compared to that which would be measured if the entire high field pattern were observed), but the overall strength is scaled down by a factor of the order of $3/4I(I+1)$.[26]

The simplest case is that of $I = 3/2$ for which the zero field time domain signal is

$$S(t_1) = \tfrac{1}{3}(3 + 2\cos\omega_Q t_1) \tag{47a}$$

with

$$\omega_Q = (e^2qQ/2\hbar)(1 + \tfrac{1}{3}\eta^2)^{1/2}. \tag{47b}$$

The existence of a single nonzero frequency in the signal function means that the principal components of the electric field gradient are not uniquely determined by the zero field spectrum of an isolated spin 3/2. On the other hand, from the viewpoint of site identification one has the conveniently simple rule that each unique ω_Q corresponds to a chemically distinct species. An illustration of this with the ^{7}Li nucleus is shown in Fig. 20 which shows the zero field spectrum of polycrystalline $Li_2SO_4 \cdot H_2O$. The two distinct sites are consistent with the structure known from x-ray diffraction and the results of single crystal NMR studies.[49]

The next simplest case is $I = 5/2$ with $\eta = 0$ for which the zero field signal function is

$$S(t_1) = \tfrac{1}{105}(53 + 32\cos\omega_Q t_1 + 20\cos 2\omega_Q t_1) \tag{48a}$$

with

$$\omega_Q = \frac{3e^2qQ}{10\hbar}. \tag{48b}$$

As η is allowed to grow, both the spacing between these two lines and their relative intensities will change. Additionally, a third sum frequency line may appear, but even for $\eta = 1$ its intensity is less than 7% that of either of the other two lines. Dipole allowed frequencies and intensities as a function of η for $I = 5/2$, 7/2, and 9/2 have been tabulated.[50]

The case of $I = 5/2$ with finite η is illustrated in Fig. 21 by the spectrum of ^{27}Al in polycrystalline potassium alum, $KAl(SO_4)_2 \cdot 12H_2O$.[51] The three distinct levels give rise to two finite frequency transitions of measurable intensity. These can be used to determine the two electric field gradient parameters of Eq. (42). In general, this is most easily done numerically. To order η^3 the frequencies are[14,40(b)]

$$\omega_Q^{5/2,3/2} = A\,[12 - (22\eta^2/9)] \tag{49a}$$

for the transition which for $\eta = 0$ corresponds to the energy difference between the $m = 5/2$ and $m = 3/2$ eigenstates, and

$$\omega_Q^{3/2,1/2} = A\,[6 + (59\eta^2/9)] \tag{49b}$$

for the transition between the $m = 3/2$ and $m = 1/2$ eigenstates. We find $e^2qQ/h = 391 \pm 2$ kHz and $\eta = 0.17 \pm 0.05$. In the highly symmetric site occupied by the aluminum atom in the alums, x-ray studies predict the lattice to be of cubic symmetry, and the aluminum nuclei are octahedrally coordinated by six water molecules.[52] The small size of the quadrupolar coupling reflects the near symmetry of the local ^{27}Al environment.

V. EFFECTS OF MOTION

Where molecules or parts of molecules are nonrigid, the spin Hamiltonians (3)–(5) described above are insufficient to provide a complete description of the observed spectral features. Under the effects of motion, the spatial terms in these Hamiltonians become time dependent and only a motionally

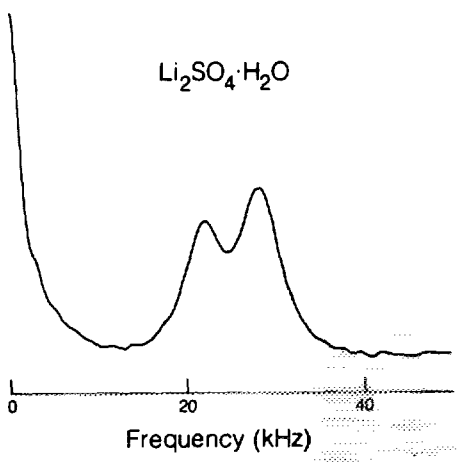

FIG. 20. Zero field ^{7}Li NQR spectrum of polycrystalline $Li_2SO_4 \cdot H_2O$. The lithium zero field evolution was sampled at 10 μs intervals for a total of 630 μs. One line (plus some nonevolving signal which appears at zero frequency) is expected for each chemically distinct site, and two such sites are observed. The zero frequency line is partially truncated for purposes of display.

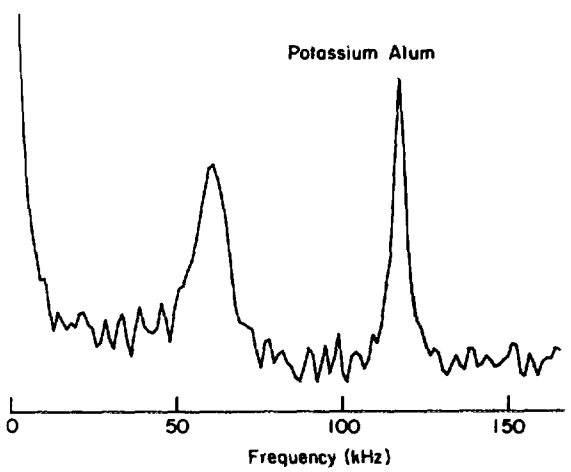

FIG. 21. Zero field ^{27}Al NQR spectrum of polycrystalline $KAl(SO_4)_2 \cdot 12H_2O$. Each spin 5/2 nucleus gives rise to a pair of zero field lines, in addition to some nonevolving magnetization which appears at zero frequency. A single such site is observed.

averaged tensor is observed. This fact is well known from high field studies, and is the basis for line shape studies of chemical exchange in solution[53] and studies of restricted motion in solids.[54] For motions which are either fast or slow (as compared to the strength of the interaction being observed) it is easy to predict the result: fast motions yield zero field spectra with sharp lines at the time-averaged value of the tensor, while very slow motions show up as discrete zero field lines at each possible value of the tensor. The intermediate case (motion or exchange at rates comparable to the magnitude of the NMR Hamiltonian) affects the line shapes, and a detailed analysis is required to solve the problem completely. Methods applicable to high field NMR are well known, and are presented by others in detail elsewhere.[54] Some consideration has been given to the intermediate regime in pure NQR.[35(e)] In this section, we will only concern ourselves with a few representative cases in the fast motion limit where a simple solution is available, and which are relevant to our experimental results. The treatment in this section closely follows the results of Bayer,[35(b)] Abragam,[40(b)] and Barnes[45] which are applicable to zero field NMR and NQR.

Where rapid motion occurs about a single axis its effect can be most simply incorporated into the expressions of the NMR and NQR Hamiltonians. As a model for these concepts, we shall consider an axially symmetric quadrupolar Hamiltonian, where the magnitude of the quadrupolar coupling is unchanged during the motion. A formally equivalent example is the dipolar coupling between two spin-1/2 nuclei.

In this section we treat four categories of motion. Three occur in a molecular frame: rapid, isotropic rotation about an axis; twofold jumps: and small librational modes. The last takes place in a lab frame: physical rotation of the sample. We start with a common approach to these types of motion. First, the static Hamiltonian is transformed from its principal axis system $(x\,y\,z)$ to a frame where the motion is described more simply (XYZ). We assume that this transformation can be accomplished by a single rotation by $\theta°$ about the y axis. In this new frame, the Hamiltonian (3) (where $\eta = 0$) can be expanded to give

$$H_Q = -A\{[3I_Z^2 - I(I+1)](3\cos^2\theta - 1)/2 + \tfrac{3}{4}\sin^2\theta(I_+^2 + I_-^2) - 3\sin\theta\cos\theta(I_XI_Z + I_ZI_X)\}. \quad (50)$$

We evaluate the time average of this Hamiltonian, for each of the motional models.

A. Rotations about a molecular axis

Allowing the molecule or molecular unit to undergo rapid rotation about the new Z axis introduces a time dependence into H_Q (or H_D). As the rotation frequency is assumed large compared to our Hamiltonian, what is actually observed is H_Q averaged over a rotational cycle. Entering an interaction frame which follows the motion of the spatial angular momentum J_Z at a frequency ω,

$$\tilde{H}_Q(t) = \langle \exp(-i\omega J_Z t) H_Q \exp(i\omega J_Z t)\rangle. \quad (51)$$

Only the first term in Eq. (50) is time independent. All other terms have zero time average over a rotational cycle. The averaged Hamiltonian which gives rise to the observed spectrum is then

$$\bar{H}_Q = -A\left(\frac{3\cos^2\theta - 1}{2}\right)[3I_Z^2 - I(I+1)] \quad (52)$$

and the averaged Hamiltonian retains the axial symmetry of the static Hamiltonian with an effective quadrupolar tensor scaled by $(3\cos^2\theta - 1)/2$. (If the local environment of the quadrupole varies during a single rotational period, and therefore the instantaneous value of the quadrupolar tensor takes on different values during that period, the averaged tensor need not be axially symmetric.[45] This is indeed the case of the CD_3 group in dimethoxybenzene, shown in Fig. 18.)

Previously we showed spectra of several compounds containing CD_3 groups. We commented that they appeared at a frequency significantly lower than do other sp^3 hybridized C–D bonds. In Fig. 22 shows an expanded view of the CD_3 methyl region in the zero field spectrum of polycrystalline perdeuterated dimethylterephthalate, whose full spectrum is shown in Fig. 15. Following the logic of Eqs. (50) and (51), the principle component of the quadrupole tensor V_{zz} is averaged to the value

$$V_{ZZ} = \tfrac{1}{2}(3\cos^2\theta - 1)V_{zz}, \quad (53)$$

where θ is the angle between the axis of rotation and the C–D bond, as shown in the figure. Assuming tetrahedral bond angles,

$$\tfrac{1}{2}(3\cos^2\theta - 1) = -0.33. \quad (54)$$

The observed quadrupolar frequency is approximately 1/3 that which characterizes other C–D bonds, as is well known from high field studies.

The structure observed in Fig. 22 again reflects the existence of dipole couplings between methyl deuterons. Due to

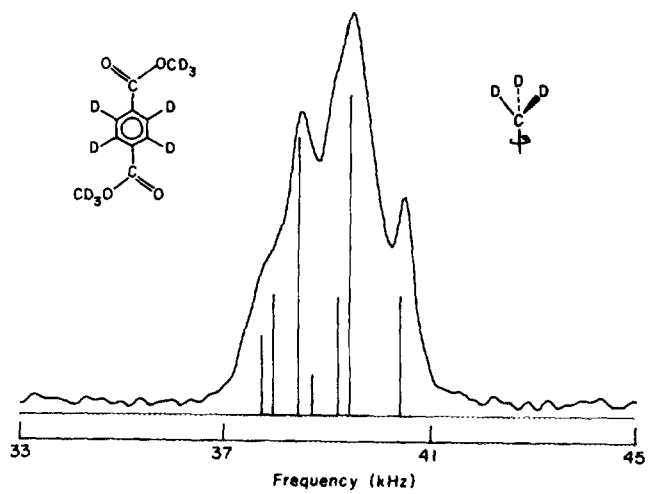

FIG. 22. Zero field ^{2}D NQR of CD_3 group of perdeuterated dimethylterephthalate. The field cycle was repeated at a rate comparable to the methyl group T_1. At this repetition rate ($\sim$ 15 s), no signal from the ring sites is observed. No η is observed for the methyl group in this compound. The structure in the spectrum is due to the dipole–dipole couplings within the methyl group: $\gamma^2\hbar/4\pi^2r^3 = 490$ Hz and $\langle r^{-3}\rangle^{-1/3} = 1.79$ Å. The seven line stick spectrum is a simulation of the effects of the dipolar fine structure superposed on the motionally averaged quadrupolar coupling.

the motion, which rapidly interchanges the spatial locations of the three individual deuterons, they are expected to have identical quadrupole coupling tensors. It is in just such a highly degenerate case that the effects of the small perturbation introduced by the dipolar coupling are expected to be most pronounced.[35(f),35(g),44] Similar spectra are observed for CD_3 groups in nematic phases of liquid crystals.[55] The precise value of the dipole coupling, and therefore the distance between deuteron nuclei, is found by modeling the complete system and taking into account the averaging caused by the motion. A simulation of the frequencies is indicated by the stick spectrum inset in Fig. 22. The ^2D–^2D internuclear distance (1.79 Å) agrees within experimental limits with the value we have previously reported for the distance between ^1H sites in the protonated analog of this molecule.[5] To accurately simulate this spectrum, we require that the dipolar and quadrupolar coupling have the same sign. In the liquid crystal studies,[55] the dipolar structure is observed with the opposite sense; i.e., simulations require that the couplings have opposite signs.

Similar effects of motional averaging are observed in zero field NMR studies of dipolar systems undergoing rapid reorientation. As before, for many coupled spins we use computer simulations. Two common examples of rapidly reorienting systems in the solid state are methyl groups and benzene, which spins rapidly about its hexad axis. In Fig. 23 we show simulated zero field and high field spectra of relatively isolated such groups. As evidence that methyl groups at room temperature are rapidly spinning, Fig. 23 should be compared to the best-resolved spectrum of Fig. 11, i.e., the dilute CH_3 group in solid sodium acetate trihydrate. In Fig. 24 we present the motionally averaged spectrum of the heteronuclear $^{13}CH_3$ group starting from three possible spin polarizations, and assuming the same sort of rapid rotation. Zero field experiments with appropriate initial conditions may be useful for separating out ^{13}CH, $^{13}CH_2$, and $^{13}CH_3$ groups in powders (cf. Figs. 13, 15, and 24).

An interesting feature obtained by averaging any rigid structure over a classical rotation about a molecule-fixed axis is that the resulting zero field Hamiltonian is isomorphic with a high field Hamiltonian with all the molecular rotation axes aligned along the field. The fast molecular rotation performs the same truncation of terms as a large Zeeman energy.

B. Discrete jumps

For jumps about the Z axis through discrete angles, the instantaneous electric field gradient tensor is calculated for each discrete orientation and a time-weighted average derived by summing over all allowed orientations.[56] For a two site jump (as executed by D_2O in many inorganic crystals at high temperature[56(a)]), and assuming that the individual sites

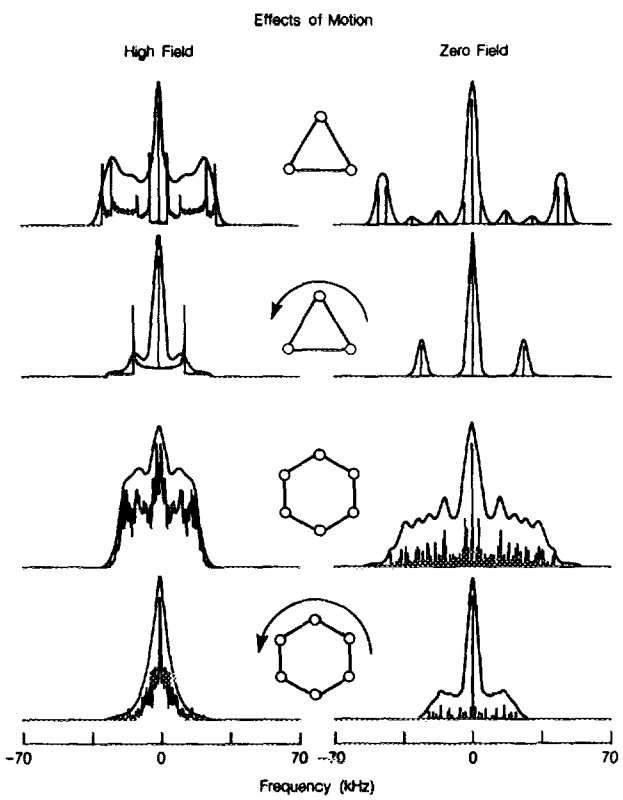

FIG. 23. High field and zero field NMR simulations for static and rapidly rotating isolated benzene rings and methyl groups. These simulations are prepared in the same manner as those of Fig. 10. For the spectra of the rapidly rotating units, the dipole–dipole coupling is averaged as in Eq. (52), and the spectra are narrowed by the motion. The prediction for the rapidly rotating methyl group agrees well with the observed spectrum of an isolated CH_3 group (cf. Fig. 12).

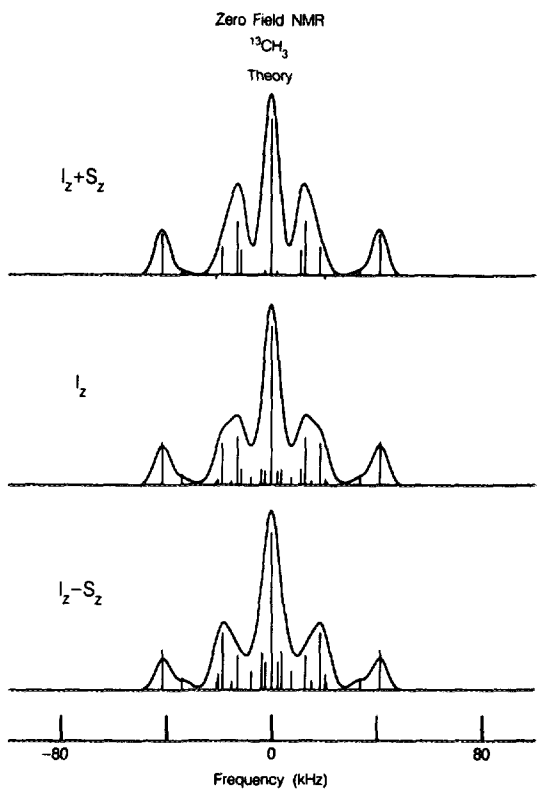

FIG. 24. Simulated zero field spectra of a rapidly spinning $^{13}CH_3$ group, as a function of initial condition prepared in high field. All C–H distances are assumed equal (1.095 Å) and all bond angles are tetrahedral. Again, the simplest zero field spectrum occurs when the initial polarizations of the two spin systems (C and H) are made equal. Spectra of ^{13}CH, $^{13}CH_2$, and $^{13}CH_3$ groups differ sufficiently (cf. Figs. 13 and 15) that zero field NMR should be able to distinguish between them.

have identical tensors related by a symmetry plane, we choose to reference our motional frame in the symmetry plane, with a Z axis along a vector which bisects the D–O–D bond angle 2θ. The first site is related to this frame via a rotation about the Y axis of θ $[R_Y(\theta)]$; the second, via $R_Y(-\theta)$. Time averaging Eq. (50) is equivalent to taking the average value of these two tensors:

$$\begin{aligned}\bar{H}_Q &= \tfrac{1}{2}(H_{Q1} + H_{Q2}) \\ &= -A\left[(3I^2_{ZM} - I(I+1)\right]\left(\frac{3\cos^2\theta - 1}{2}\right) \\ &\quad + \tfrac{3}{4}\sin^2\theta\left[(I^2_{+M} + I^2_{-M})\right]. \end{aligned} \tag{55}$$

Even if the tensors of the static sites are equivalent and axially symmetric, in the averaged tensor the coefficient of the term $(I^2_{+M} + I^2_{-M})$ need not vanish and the motion introduces not only an apparent shrinkage in the magnitude of the quadrupolar tensor but also a marked departure from axial symmetry. [For specific values of θ, the axis system in the new frame may need to be relabeled to conform with the conventional notation of Eq. (42).] For $2\theta \sim 109.5°$ (the tetrahedral angle), $\eta \sim 1$. Such motionally induced asymmetry parameters have been observed in zero field NQR and will appear in a later work.[57]

C. Torsion and small librations

As a final simple example of molecular motion in zero field, we consider the effect of small amplitude torsional or librational modes.[35(b)] These are modeled by allowing Z to represent the equilibrium or average orientation of the tensor, and introducing small rotations about the y axis of θ radians. For small θ and to lowest nonvanishing order in θ we can expand Eq. (50) in powers of θ as

$$\begin{aligned}\tilde{H}_Q(t) = -A\Big\{&\left(1 - \frac{3\theta^2}{2}\right)\{3I^2_Z - I(I+1)\} \\ &+ \tfrac{3}{4}\theta^2(I^2_+ + I^2_-) - 3\theta(I_XI_Z + I_ZI_X)\Big\}. \end{aligned} \tag{56}$$

Averaging over θ to get the time-averaged Hamiltonian $\bar{H}_Q$, this last term disappears and we rewrite $\bar{H}_Q$ as

$$\begin{aligned}\bar{H}_Q = -A\Big\{&\left(1 - \frac{3\,\overline{\theta^2}}{2}\right)[3I^2_Z - I(I+1)] \\ &+ \tfrac{3}{4}\bar{\theta}^2(I^2_+ + I^2_-)\Big\}, \end{aligned} \tag{57a}$$

where

$$\overline{\theta^2} = \langle\theta^2(t)\rangle. \tag{57b}$$

This corresponds to a scaled quadrupolar coupling constant and an asymmetry parameter of $\eta = \frac{3}{2}\,\overline{\theta^2}$. By a similar treatment, dipolar tensors can develop an asymmetry.[58] In two-spin heteronuclear spin-1/2 systems with such an asymmetric dipolar tensor (and therefore no degenerate energy levels) *all 12 lines* predicted by Eq. (30) should be observed.

For each of these molecular frame motions, the averaged tensor may have different value and symmetry than the static tensor. Examples of motions resulting in small η in dipolar coupled systems will also be given in a future work.[57] It is important to note that all the types of motion we have discussed are homogeneous, in the sense that we assumed that all crystallites undergo the same type of motion independent of their orientation in the lab frame. Therefore, the resulting spectra retain the sharp features of zero field NMR of static samples; no broadening is introduced unless the motional behavior is itself inhomogeneous over the sample. It is possible such inhomogeneity may be the source of the broad features in the ^{2}D NQR of lauric acid (Fig. 19).

D. Sample rotation

As a final example of the effects of motion on zero field spectra, we consider the effects of bulk sample rotation on zero field spectra. This type of motion differs from those described above in that the axis of rotation differs for each crystallite orientation in a fixed lab-based frame of reference. We proceed as above and transform into a lab-based frame as in Eq. (50), where the angle θ is now orientation dependent. For fast rotation and only homonuclear couplings, the averaging in Eq. (51) is mathematically identical to that observed upon entering the rotating frame of high field NMR studies; this is a consequence of Larmor's theorem, and

$$\bar{H}_Q = -A\left(\frac{3\cos^2\theta - 1}{2}\right)[3I^2_Z - I(I+1)], \tag{58}$$

where θ is now referenced to a laboratory frame. Thus the zero field spectrum of an isolated deuteron or two spin-1/2 system will broaden into the powder pattern illustrated at the bottom of Fig. 1. For most systems, practical sample rotation rates will be too slow for this simple treatment to apply. The primary effect of the rotation will be to cause some broadening in the observed line features. A combination of sample spinning at frequency ω_r and a magnetic field B such that $\omega_r = \gamma_i B$ will produce an untruncated Hamiltonian H_D or H_Q, and thus a normal zero field spectrum, in rough analogy to the cancellation of nutation and sample rotation in high field.[29] This should be useful for distinguishing between nuclear spins of heteronuclear systems (e.g., ^{2}D–^{1}H), and for the purposes of spin decoupling in zero field spectroscopy.

VI. EXPERIMENTAL DETAILS

A. Zero field interval

This section gives design criteria and a brief description of the experimental apparatus and procedure. Complete details can be found elsewhere.[46] The distinctive aspect of the present field cycling schemes is that the evolution of coherence is induced and terminated by the sudden removal and reapplication, respectively, of a large static field, or by the application of short dc field pulses in conjuction with adiabatic demagnetization and remagnetization in the laboratory frame.

1. Timing considerations

There are several practical criteria for measuring an interferogram in this way. The first crierion is that the switching must take place sufficiently rapidly that coherence does not decay. This may be coherence prepared before the

switching, or, more often, terms in the density operator which become time dependent as a consequence of the rapid switching between Hamiltonians. Thus the switching time τ_s from a condition of high field to zero field should satisfy $\tau_s \ll T_2$. If the spectrum has resolved line structure, then its spectral width is roughly characterized by the square root of its second moment M_2, which satisfies the condition $M_2^{-1/2} < T_2$. A useful criterion, then, is that $\tau_s \ll M_2^{-1/2}$; i.e., negligible evolution due to the internal Hamiltonian occurs during switching. Truly instantaneous switching would require $\tau_s \ll 1/\omega_0$, where ω_0 is the Larmor frequency in the switched field, but Larmor precession during the rise and fall of the field does not destroy coherence and should be of no consequence as long as it is reproducible.

2. Field cycling

For many systems of interest $\tau_s \cong 10^{-6}$ s suffices. Switching on this time scale is difficult for the fields of $\gtrsim 1$ T which are desirable for creating a large equilibrium magnetization and high Larmor frequency for sensitive detection in t_2. Mechanical translation of the sample to and from the field region on this time scale also appears impractical. An idealized scheme for incorporating the advantages of large polarizing and observation fields, and simultaneously satisfying the rapid switching criterion, is to lower and raise the fields in two steps. This is illustrated in Fig. 25. We will refer to the notation of Fig. 25 throughout this section. The sample is magnetized in the largest available field. Then, it is transported to an intermediate field $B_{\rm int}$ with Larmor frequency $\omega_{\rm int} = \gamma B_{\rm int}$ which still satisfies $\omega_{\rm int} \gg M_2^{1/2}$. (For most dipolar coupled systems, an intermediate field of ~ 0.01 T is sufficient.) This step need only be completed in a time $\lesssim T_1$ and is conveniently accomplished by mechanical translation of the sample (~ 75 cm), which in our apparatus takes ~ 150 ms in either direction.

An alternative approach would be to execute the field cycle instead by two electronic steps. Variable field T_1 spectrometers are designed to allow for rapid ($\sim$ms) variation of large fields (~ 1 T) purely by electronic means.[59] While the initial polarization level and detection sensitivity may suffer due to the lower value of B_0, for samples with short T_1's the decrease in cycle time should compensate in part for the smaller applied fields.

3. Sample container

The sample is contained in a cylindrical shatter-resistant plastic holder (Kel-F for experiments on ^{1}H containing systems, otherwise nylon) about 2 cm in length. The sample tube fits snugly inside a 10 mm o.d. thin-walled glass tube of length ~ 75 cm, which extends from a standard rf coil in the bore of a 4.2 T solenoidal superconducting magnet B_0 to a region below the magnet cryostat where the fringe field due to B_0 is equal to the desired intemediate field (0.01–0.04 T). Positive or negative air pressure applied at the lower end of the tube causes the sample to shuttle up and down. Its position at either end is fixed by plastic stops. All of the experiments reported here were performed at room temperature.

4. Zero field region

At the lower position is the region of zero field. A pair of electromagnets (B_1 and B_2) are wound to provide the time-varying fields of the order of the fringe field due to B_0. (Additional unswitched shim coils can provide a finer adjustment of the actual value of the residual fields.) The first magnet (B_1) is designed to accurately negate the fringe field and produce a sizable volume of near-zero magnetic field. This coil is referred to as the "bucking coil." The second electromagnet (B_2) is smaller and encloses the glass shuttle tube. It is designed to be rapidly switched and is the source of the experimental sudden switching. In principle, a single magnet coil

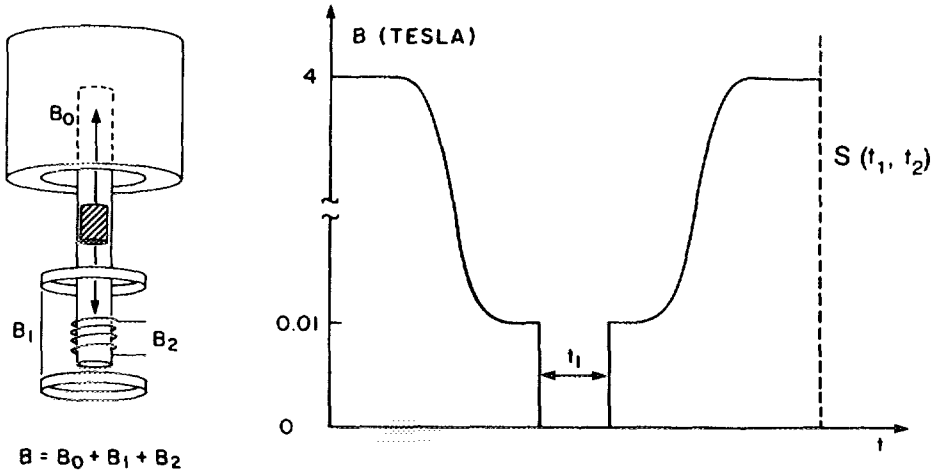

FIG. 25. Schematic of the field cycling technique. Left: the three main magnet coils. B_0 is the superconducting solenoid of the high field NMR spectrometer. B_1 is a large ($\sim$ 12 cm diam) electromagnet wound to cancel the fringe field due to B_0 at a position ~ 50 cm below the cryostat (~ 0.01 T). B_2 is a much smaller electromagnet (~ 1.5 cm diam) and is capable of being rapidly (< 1 μs) switched off and on. Right: the time dependence of the applied magnetic field, as experienced by the sample. The sample begins in the large applied field of the superconducting magnet B_0. As it moves from the bore, the field gradually decreases to a value ~ 0.01 T. Then electromagnets B_1 and B_2 are suddenly switched. The field rapidly doubles in size (not shown), and more slowly decreases back to ~ 0.01 T. B_2 is then shut off, and evolution is initiated. At the time t_1, B_2 is turned back on, and evolution is terminated. First B_1 and then B_2 are turned off, and then the sample is returned to the bore of B_0 where the amplitude of the evolved magnetization is detected.

might be designed to serve both functions (i.e., rapid switching and high homogeneity); practically, however, such a unified approach implies intolerable demands on the electronics. This two-coil setup does pose one complication, however. B_1 nulls the fringe fields over a large volume of space. Were it energized continuously, the sample would pass through a field-free region during transit before feeling the effects of the switching coil B_2. To overcome this, the bucking coil, too, must be switched. This insures that the sample always remains in an applied field $B_{\text{applied}} \gg B_{\text{loc}}$ until the sudden transient which initiates evolution. If B_{applied} is not much larger than B_{loc}, then at the intermediate field the system will be in mixed eigenstates of the high and zero field Hamiltonians. After switching, evolution is still restricted to the same frequencies; however, the amplitude of the oscillating signal will be decreased by the extent of the mixing.

5. Specifics of the field cycle

The field cycle (for concreteness, all switching times and fields are referenced to the apparatus as designed to measure dipolar couplings) is composed of the following steps:

(1) The sample is polarized for a time $\sim T_1$ in high field.

(2) A three-way gas valve is switched. Negative pressure applied to the glass tube causes the sample to move from the bore into position in the zero field region. At all times during transit (~ 150 ms), the sample resides in the fringe field due to B_0 (> 0.01 T).

(3) Both coils (bucking and switching) are simultaneously energized. The switching coil B_2 adds a field equal and parallel to the fringe field and so the applied field rapidly (~ 300 ns) approaches ~ 0.02 T. Simultaneously, the bucking coils B_1 is energized (~ 10 ms switching time). As its field is antiparallel to the fringe field of B_0, the applied field slowly returns nearly to its initial (~ 0.01 T) value. At all times, the spins are in fields greater than the local field and the nuclear magnetization is unaffected by these time-varying fields.

(4) The switching coil B_2 is quenched. Zero field evolution is initiated. At the time t_1 (as determined by the 10 MHz clock which synchronizes all operations of the high field spectrometer), the switching coil is reenergized. The evolved magnetization is stored.

(5) The bucking coil is switched off.

(6) Pressure is applied at the sample, and it returns to high field.

(7) The amplitude of the evolved magnetization is sampled.

6. Homogeneity of the zero field region

Small residual fields are truncated by the larger local fields and contribute to zero field linewidths only in second order. These residual fields can be shimmed to negligible size ($< 10^{-6}$ T) on heteronuclear liquid samples. For a single I–S pair and an indirect dipolar coupling J, the zero field free induction decay is

$$M_z(t_1) = \tfrac{1}{2}(b_I + b_S) \pm \tfrac{1}{2}(b_I - b_S)\cos(Jt_1), \tag{59}$$

where, as before, the $+$ sign holds when the more highly polarized are detected, and the $-$ sign otherwise. As the natural linewidths in liquid samples are $\sim$Hz, and any additional linewidth is indicative of the field inhomogeneity, these samples provide a convenient measure of the residual fields.[30] In most applications, residual fields as large as 10^{-5} T (which can be achieved using only a commercial gaussmeter as a probe) produce no discernable effect on the zero field spectrum.

B. High field detection sequences

The high field detection circuits used to detect the high field magnetizations are based on standard designs incorporating a gapped solenoid wrapped around the shuttle tube. The same coil is used for both excitation and detection. Various familiar rf pulse sequences are used. The simplest possibility [Fig. 26(a)] is to give a single $\pi/2$ pulse and record the resulting free induction decay in t_2. Frequently, experimental difficulties associated with "dead time" (the finite time it takes for the receiver circuitry to recover after a strong rf excitation pulse) make it preferable to record the free induction decay after a solid echo sequence[60] [Fig. 26(b)]. There is effectively no dead time in the zero field interval t_1. Both of these sequences suffer from the disadvantage that the transverse magnetization decays in a characteristic time $M_2^{-1/2}$ (10–100 μs). More complicated pulse sequences are known which eliminate evolution under the influence of the homonuclear dipole–dipole couplings and greatly extend the lifetime of the transverse magnetization[61,62] The prototype of such sequences is the WAHUHA four pulse cycle[61(a)] illustrated in Fig. 26(c). A preferable sequence (because it is technically less demanding) is the pulsed spin-locking experi-

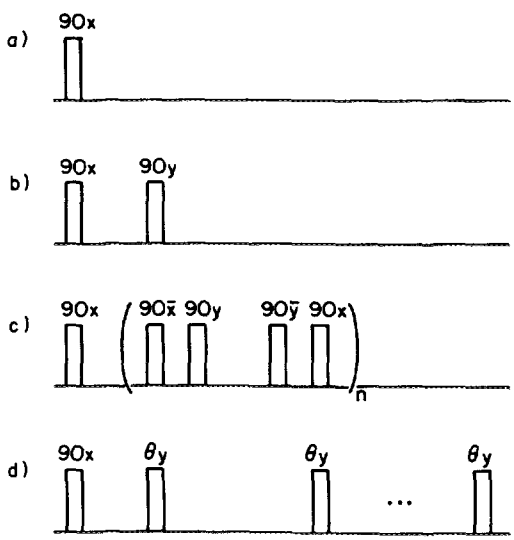

FIG. 26. Pulse sequences for the high field detection of zero field NMR. (a) 90° pulse initiates evolution. The high field free induction decay is sampled as soon after the pulse as possible. (b) Solid echo sequence. The second pulse causes a refocusing of the magnetization, forming an echo. This allows the magnetization to be sampled at a time many μs after the pulse and alleviates experimental problems with dead time. (c) Multiple pulse sequence (WAHUHA). Sampling in the windows after every fourth pulse yields the high field chemical shift spectrum. (d) Pulsed spin locking (or multiple echoes). After each pulse, the magnetization can be sampled. For dipolar coupled systems, $\theta = 45°$ minimizes the decay. For quadrupolar systems θ is chosen empirically. For experiments on ^{2}D, $\theta \sim 80°$ frequently appears optimal.

ment of Fig. 26(d).[62] This simple sequence forfeits high field information in order to minimize the signal decay and thus maximize the accumulated signal energy in t_2 (subject to the constraints of $T_{1\rho}$). The signal at a given time in t_1 is then taken as the average of all point samples in the multiple-pulse train. Significant increases in signal-to-noise ($\sim$5–50) may be achieved by this technique.

VII. EXTENSIONS AND CONCLUSION

A. Two-dimensional high field–zero field correlations

Figure 27 shows the two-dimensional zero field–high field correlation spectrum of polycrystalline $Ba(ClO_3)_2 \cdot H_2O$. The high field signal after a solid echo sequence is observed as a function of the zero field time t_1, and the signal function $S(t_1,t_2)$ is subjected to a real Fourier transform with respect to both time domains. The projections onto the ω_1 and ω_2 axes show the zero field and high field spectra, respectively. The cross peaks in the two-dimensional spectrum show the correlations between the low field and high field spectra. Portions of the high field spectrum at the edges of the spectrum, where the internuclear vector is nearly parallel to the applied field, correspond to the nonevolving components of the zero field spectrum. The singularities in the high field powder pattern, where the internuclear vector is perpendicular to the field, are accentuated in slices corresponding to the finite frequency parts of the zero field spectrum. This corresponds precisely to the description presented in the Introduction.

In heteronuclear I_n–S systems (e.g., $I = {}^1H$, $S = {}^{13}C$) either spin reservoir should reveal identical ω_1 frequencies, and the choice of the observed nucleus is based on other considerations. Normally, signal-to-noise is better for the spin system with larger γ (e.g., the protons). If, however, the high γ (^1H) nuclei are abundant and strongly coupled to one another, it may be difficult to observe the heteronuclear lines amidst the much stronger background of ^1H–^1H couplings. Then, in the spirit of separated local field spectroscopy,[24,25] one should observe the rare spins. It should be possible to get the best of both worlds; the signal-to-noise advantage of the I nucleus with the selectivity of the rare S spins. First, polarize the S spins by whatever means possible in high field. Before initiating the field cycle, saturate the I spin magnetization. At the end of t_1, the only I-spin magnetization available to be observed must arise from those I spins strongly coupled to S spins.

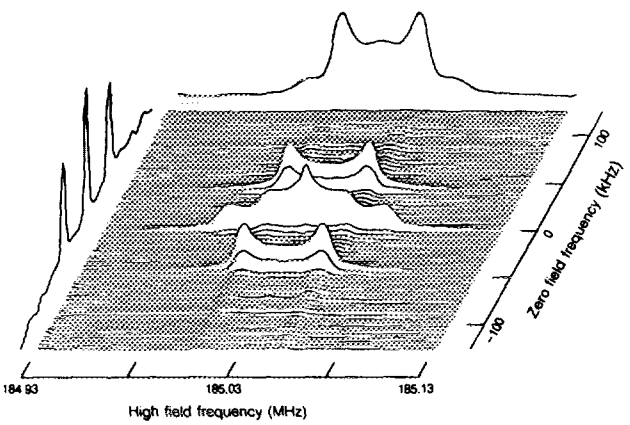

FIG. 27. Two-dimensional zero field–high field dipolar correlation spectrum of polycrystalline $Ba(ClO_3)_2 \cdot H_2O$. For each of 64 values of t_1, the zero field interval, the high field free induction decay after a solid echo sequence is accumulated and stored. A double real Fourier transform in t_1 and t_2 is applied to the signal $S(t_1, t_2)$. At the left and top are the projections of the zero field and high field spectra. In the center, the correlations between the two frequency domains. Signals which appear at zero frequency in ω_1 correlate most strongly with signals from orientations of the two-spin system which are nearly at the edges of the high field powder pattern. Zero field signals which appear at $\pm \sim 42$ kHz correlate to orientations which appear near the peaks (at $\pm \sim 21$ kHz) of the high field powder pattern.

As the motivation for the zero field experiment is that the high field dipolar and quadrupolar powder patterns are broad, often featureless, and largely devoid of information, it will rarely prove useful to accumulate a normal free induction decay in t_2. As long as the same Hamiltonians (dipolar and/or quadrupolar) govern the dynamics of both time periods, ω_2 contains the same information as ω_1, only at much lower resolution. Two options, then, are available: First, one might modify the high field portion of the spectrum such that t_2 evolution is governed by a more tractable Hamiltonian. For example, techniques for the measurement of chemical shifts in powders are well known. Dipolar couplings in zero field might thus be correlated to the high field chemical shifts. In homonuclear systems, dipolar decoupling sequences such as WAHUHA, MREV-8, or their more sophisticated relatives[61] extract chemical shift patterns in strongly coupled systems. For rare spin species such as ^{13}C, proton decoupling should suffice to correlate untruncated couplings with chemical shift patterns. Unfortunately, the chemical shift anisotropy severely degrades the chemical sensitivity of such an experiment.

The ideal zero field experiment would incorporate high resolution in the high field detection period, such as is accomplished by magic angle sample spinning, to provide correlations between chemically distinct sites and geometric factors. Practical considerations make such an experiment difficult. Rotation about a laboratory-fixed axis during the zero field period (Sec. VI D) reintroduces powder broadening in zero field, and high speed spinning inserts ($\sim$3 kHz) are not readily started and stopped. In homonuclear systems, one can compensate by cycling not to zero field but a small field whose magnitude and direction are adjusted to precisely null the effects of the spatial rotation. No such adjustment can be made in heteronuclear spin systems, where magic angle spinning (in conjuction with higher power decoupling) is most useful. Magic angle hopping[63] should prove more useful.

B. Two-dimensional zero field–zero field experiments

Deuterium NQR spectra (Figs. 16–18) in zero field show the sort of high resolution features most often associated with high resolution solution state NMR. The quadrupolar couplings identify chemical environment (like a chemical shift), while the dipole–dipole couplings correlate near neighbors in space (while J couplings correlate near neighbors through bonds). This suggests correlation experiments of the sort common in solution state two-dimensional NMR (such as NOESY[64]). Level crossing experiments utilize

"double transitions" to correlate neighboring deuterons, and to attempt to assign transitions to sites in solid.[44(c),65] A time domain version of this type of correlation experiment is shown in Fig. 28. Here we allow for two independent zero field time intervals t_1 and t_2. The signal is detected in high field during yet a third time period.

The zero field times t_1 and t_2 are independently incremented. The mixing period where large dc fields are applied separates the two periods and is kept fixed. Two-dimensional Fourier transformation yields a matrix. Correlations show up as off-diagonal peaks in the two-dimensional spectrum. For short mixing times, we expect correlations only between transitions corresponding to a single site. For long field pulses ($\sim$1 ms), spin diffusion between sites becomes allowed and the crosspeaks may indicate spatially neighboring sites. They may also correspond to chemical exchange between sites during the mixing period.

These experiments, like the magic angle hopping zero field correlation experiment, may become quite lengthy. We are currently working at demonstrating several less time-consuming versions of these and other zero field correlation experiments.[66]

C. Alternative initial conditions

In the experiments considered so far the density operator just prior to the zero field period has been proportional to some linear combination of nuclear magnetizations. Starting from magnetization, the spectra observed are subject to dipole selection rules [as expressed by Eq. (18)]. The molecular frame operators which determine the selection rules are of the same rank as the initial density operator. For systems of many levels, however, there are other experimentally accessible forms of nuclear order. One might wonder whether or how these alternative states might be used to advantage. The frequencies obtainable by Fourier transformation of some observable with respect to the period of free evolution in zero field, t_1, will always be some subset of the differences between the eigenvalues of H_M. The question, then, is how to control the amplitudes of these Fourier components and enhance the information content of the spectrum. Some simple examples of preparation sequences designed with the intent of spectral editing were presented in our discussion of heteronuclear spin systems (Sec. III C). The problem, in fact, is much more general.

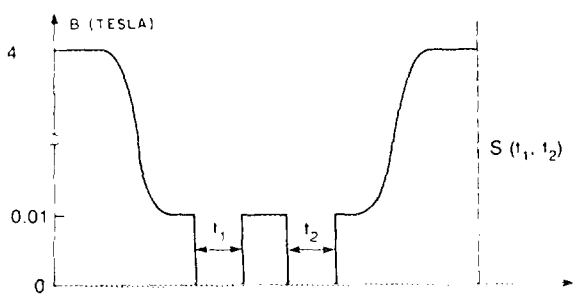

FIG. 28. Two-dimensional zero field–zero field correlation experiment. In quadrupolar systems, the quadrupolar frequencies label individual sites while doplar couplings provide connectivities between sites.

1. Changing the selection rules

As noted in Sec. IV C, half-integral quadrupolar spins often have appreciable dipole intensity only in the lines which are characterized by $n_M = \pm 1$. For a nucleus with $I = 5/2$ and more that one distinct chemical environment, observation of the $n_M = 2$ sum frequency line should aid in assigning the two normal $n_m = 1$ lines to a particular site, just as the difference frequency ν_0 lines were used in analyzing the $I = 1$ systems of Sec. IV A and Fig. 18. In order to break the dipole selection rule, the tensor rank of the prepared operator must be greater than $l = 1$. Sequences are known which to a good approximation prepare and detect high field dipolar or quadrupolar order,[67] which is a rank $l = 2$ operator. By inserting a field cycling period in between such preparation and detection, the three $l = 1$ autocorrelation functions are replaced in Eqs. (12) and (13) by five $l = 2$ autocorrelation functions, giving "quadrupolar" selection rules.

2. Initiation of evolution by dc pulses

A simpler method of achieving a similar result is to simply decrease the field at the sample adiabatically all the way to zero. This leaves the nuclear order stored in some combination of the population differences between states of H_M, which generally correspond to higher rank operators.[68] Coherent evolution in zero field can thereafter be initiated by a brief magnetic field pulse. These pulses can be selective in either of two senses: First, they may be tuned to a particular NQR frequency which may thereafter be directly detected.[69] Or, strong dc pulses may be used to initiate and store evolution at all transitions simultaneously. These dc pulses may be made selective by choosing to apply a pulse of length τ so that evolution is initiated for one spin species but not another.[12(a)] For systems with small coupling constants, it will generally be preferable to apply a second pulse and store some portion of the time evolved density operator as population differences which can be detected with higher sensitivity in high field, after adiabatic remagnetization. This experiment is closely related to field cycling with sudden switching, and an example of such a field cycle is shown in Fig. 29.

Where an accurate intensity calculation is essential to an interpretation of the observed spectrum, as in the study of dipolar coupled spin-1/2 systems, it will be difficult to closely match the observed zero field intensities after adiabatic demagnetization as the initial state and detected operator depend strongly on the details of the field cycle. Moreover, the preparation sequence is rarely equally effective for all power orientations, even for the high field methods described above. This introduces an explicit Ω dependence into the initial and final density operator [Eq. (6)], and therefore such adiabatic field cycles result in complicated and generally unpredictable equations for the intensities.

In quadrupolar systems, however, this sort of experiment has considerable advantages over the sudden switching experiment. Quadrupolar fields ($\sim$0.03–0.1 T) tend to be

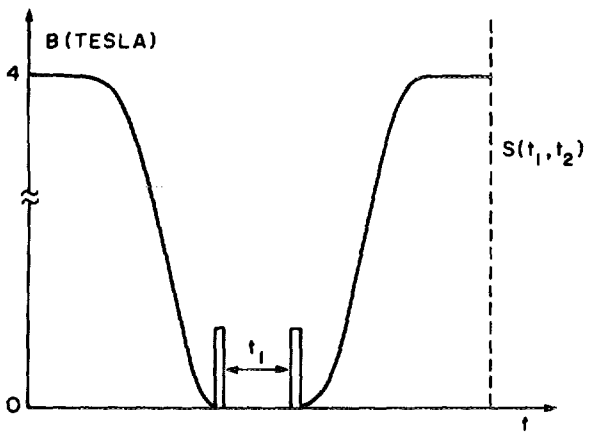

FIG. 29. Alternative field cycling scheme. Adiabatic demagnetization to zero field is followed by a short, intense dc field pulse to initiate evolution. At the end of t_1, a second dc field pulse stores some of the evolved spin order as population differences. The sample is then remagnetized to high field, and the evolution of the magnetization under the new zero field selection rules probed in high field. If level crossings between nuclear spin species occur during the transit to and from zero field, then magnetization may be transferred between spin species. This allows for indirect detection of the zero field time domain signal of one spin species by its effect on a second.

much larger than dipolar fields ($\sim$0.001 T). As the necessary switching fields become larger, the associated electronics becomes bulkier, more expensive, and significantly more hazardous, particularly where the timing sequence (see above) requires many ms of intense fields. Here, only two short ($\sim\mu$s) pulses are used, which makes design of the zero field apparatus significantly simpler. The absolute intensities of specific lines are less important, and the restrictive dipolar selection rules are overcome. Additionally, we can capitalize on the adiabatic cycle and adapt the level-crossing schemes of Hahn and others[8–10] to time domain experiments. This is particularly valuable for quadrupolar spin systems where the high field T_1's may be inconveniently long. During the demagnetization, the sample passes through values of the externally applied field where energy splittings for two different nuclear spin species may be instantaneously matched. If these two species have different polarizations and are coupled by a dipolar interaction, polarization may be transferred from a rapidly relaxing site to a more sluggish neighbor; or, from an abundant, high γ, short T_1 nucleus like ^{1}H to some less sensitive species. Experiments based on this idea have been reported elsewhere.[12(a)]

D. Direct detection in zero field

Clearly, in order for the most powerful experiments to become routine, it will be necessary to develop a method for direct obsevation of the oscillating magnetization in zero field. The method should be capable of high sensitivity and have a detection efficiency which is frequency independent. This rules out any rf detectors based on Faraday's law devices, where a voltage is induced proportional to the frequency of oscillation.

Just such a device in fact exists. The superconducting quantum inteference device (SQUID) is an ultralow noise rf flux detector. It has recently been used in the detection of spin noise, i.e., the random fluctuations in polarization of a macroscopic ensemble of nuclear spins,[70] and is certainly sufficiently sensitive for the direct observation of an oscillating magnetization in zero field.[16(a),71] We are currently exploring the possibility of incorporating SQUID detectors into our zero field apparatus. Their high sensitivity may alleviate the need for a large polarizing field. More importantly, those experiments described above (e.g., chemical shift-dipole coupling correlation by magic angle hopping combined with zero field NMR, or two-dimensional zero field correlation experiments) which have been described as three-dimensional become instead two-dimensional. This results in a substantial reduction in the minimum experimental time.

E. Other low and zero field studies

Field cycling methods are often used in variable field studies of nuclear T_1's. There are a number of other applications where field cycling might profitably be used to ease difficult experimental requirements or enhance information content. In NMR studies of metals[72] or small molecules adsorbed on metallic surfaces[73] the Knight shifts may be a sizable fraction ($\sim$1%) of the resonance frequency. At high fields, the necessary excitation and detection bandwidths are far beyond the capabilities of most NMR spectrometers. These problems might be largely overcome by working at lower fields. For example, one might use a large field to build up a large polarization, smaller fields during the excitation and detection periods, and ultrahigh sensitivity detectors to observe the signal. Field cycling methods should also prove of advantage in studies of spin absorption in low fields, including the observation of spin absorption at multiples of the Larmor frequency.[7,9(a),36,74]

Using field cycling techniques one might study the dynamics of ordering and disordering in liquid crystals in a magnetic field. In some of these ordered phases (e.g., smectic *C* or cholesteric phases) the director cannot be aligned by an external field and therefore only powder patterns are observed in high field. Zero field NMR should provide the same sort of resolution associated previously only with NMR spectra of nematic phases.

ACKNOWLEDGMENTS

D. B. Zax was supported by a National Science Foundation Graduate Fellowship, and K. W. Zilm by an IBM postdoctoral fellowship. We gratefully acknowledge M. Mehring for helpful conversations, H. Zimmerman for synthesizing many of the deuterated molecules, and J. Murdoch for writing several of the computer simulation routines. This work was supported by the Director, Office of Energy Research, Office of Basic Energy Sciences, Materials Science Division of the U.S. Department of Energy and by the Director's Program Development Funds of the Lawrence Berkeley Laboratory under Contract No. DE-AC03-76SF00098.

APPENDIX A

In this Appendix we will take a somewhat different approach to the solution of Eq. (16) for the case of two homonu-

clear dipolar spin-1/2 nuclei, or, equivalently, an isolated spin-1 system. Rather than calculating only the signal function, we will explicitly represent the lab frame density matrix $\rho_L^{\Omega}(t_1)$. This corresponds to following the evolution of the lab frame magnetization at each orientation of the powder at all times.

While it is always possible to represent the density matrix as a set of numbers, greater physical insight is gained if we instead choose a basis set of spherical tensor operators, in the spirit of the various fictitious spin-1/2 formalisms which have recently appeared in the literature.[75] Generally, an $N \times N$ traceless Hermitian matrix requires $N^2 - 1$ one of these operators. For the special case of the two identical spins, we can somewhat simplify the bookkeeping at the start. No matrix elements of any tensor operators couple the singlet state with the triplet manifold. Formally, the problem is identical to that of an isolated spin-1, and the eight operators chosen as a basis set in Table A1 are intimately related to the operator formalism of Vega and Pines.[75(a)]

While we are interested in the evolution of the prepared state in the laboratory frame, the evolution operator $\exp(iHt)$ is not readily applied in this frame. The quantity we wish to calculate is, instead

$$\rho_L^{\Omega}(t) = R^{-1} \exp(-iH_M t_1) R \rho_L^{\Omega}(0) R^{-1} \exp(iH_M t_1) R. \tag{A1}$$

This calculation may be viewed alternatively as rotating the evolution operator into the basis set of the high field density operator, or instead as first rotating the density operator into the molecular frame, appending the evolution operator, and returning to the lab frame. We will adopt the latter perspective. Repeating the first few steps of Sec. II B 5,

$$R\rho_L^{\Omega}(0)R^{-1} = I_{zM}\cos\beta - I_{xM}\sin\beta\cos\alpha + I_{yM}\sin\beta\sin\alpha. \tag{A2}$$

In Table A1, we give explicit representations for these operators in the eigenbasis of the Hamiltonian. As an example, the time evolved matrix $I_{xM}(t_1)$ is given in Table A2. More generally, for the triplet manifold of two identical spins (or a real spin-1 system) in the basis set of Table A1,

$$I_{xM}(t_1) = I_{xM}\cos\omega_{23}t_1 + (I_{yM}I_{zM} + I_{zM}I_{yM})\sin\omega_{23}t_1, \tag{A3a}$$

$$I_{yM}(t_1) = I_{yM}\cos\omega_{31}t_1 + (I_{xM}I_{zM} + I_{zM}I_{xM})\sin\omega_{31}t_1, \tag{A3b}$$

and

$$I_{zM}(t_1) = I_{zM}\cos\omega_{12}t_1 + (I_{xM}I_{yM} + I_{yM}I_{xM})\sin\omega_{12}t_1. \tag{A3c}$$

Transforming back into the lab frame, the time evolved density matrix at a time t_1 is, in terms of the lab-based tensors

TABLE A1. Eigenstates, eigenvalues, and operator representations for three-level systems.

Triplet manifold of two coupled spin-1/2 nuclei

$|1\rangle = -\frac{i}{2^{1/2}}(|\alpha\alpha\rangle - |\beta\beta\rangle)$ $\quad |2\rangle = \frac{1}{2^{1/2}}(|\alpha\alpha\rangle + |\beta\beta\rangle)$

$|3\rangle = \frac{1}{2^{1/2}}(|\alpha\beta\rangle + |\beta\alpha\rangle)$

$\langle 1|H_D|1\rangle = \langle 2|H_D|2\rangle = -\frac{1}{2}\omega_D$ $\quad \langle 3|H_D|3\rangle = \omega_D$

$I = 1$

$|1\rangle = -\frac{i}{2^{1/2}}(|+1\rangle - |-1\rangle) = |-\rangle$ $\quad |2\rangle = \frac{1}{2^{1/2}}(|+1\rangle + |-1\rangle) = |+\rangle$

$|3\rangle = |0\rangle$

$\langle 1|H_Q|1\rangle = -A(1-\eta)$ $\quad \langle 2|H_Q|2\rangle = -A(1+\eta)$ $\quad \langle 3|H_Q|3\rangle = +2A$

I_z	$\|1\rangle$	$\|2\rangle$	$\|3\rangle$
$\langle 1\|$	0	i	0
$\langle 2\|$	$-i$	0	0
$\langle 3\|$	0	0	0

$I_x I_y + I_y I_x$	$\|1\rangle$	$\|2\rangle$	$\|3\rangle$
$\langle 1\|$	0	1	0
$\langle 2\|$	1	0	0
$\langle 3\|$	0	0	0

$I_x^2 - I_y^2$	$\|1\rangle$	$\|2\rangle$	$\|3\rangle$
$\langle 1\|$	-1	0	0
$\langle 2\|$	0	1	0
$\langle 3\|$	0	0	0

I_x	$\|1\rangle$	$\|2\rangle$	$\|3\rangle$
$\langle 1\|$	0	0	0
$\langle 2\|$	0	0	1
$\langle 3\|$	0	1	0

$I_y I_z + I_z I_y$	$\|1\rangle$	$\|2\rangle$	$\|3\rangle$
$\langle 1\|$	0	0	0
$\langle 2\|$	0	0	$-i$
$\langle 3\|$	0	i	0

$3I_z^2 - I(I+1)$	$\|1\rangle$	$\|2\rangle$	$\|3\rangle$
$\langle 1\|$	1	0	0
$\langle 2\|$	0	1	0
$\langle 3\|$	0	0	-2

I_y	$\|1\rangle$	$\|2\rangle$	$\|3\rangle$
$\langle 1\|$	0	0	1
$\langle 2\|$	0	0	0
$\langle 3\|$	1	0	0

$I_x I_z + I_z I_x$	$\|1\rangle$	$\|2\rangle$	$\|3\rangle$
$\langle 1\|$	0	0	i
$\langle 2\|$	0	0	0
$\langle 3\|$	$-i$	0	0

TABLE A2. Time evolution of I_x.

$$I_x(t) = \begin{pmatrix} 0 & 0 & 0 \\ 0 & 0 & \exp(i\omega_{32}t) \\ 0 & \exp(i\omega_{23}t) & 0 \end{pmatrix}$$
$$= \begin{pmatrix} 0 & 0 & 0 \\ 0 & 0 & \cos\omega_{23}t \\ 0 & \cos\omega_{23}t & 0 \end{pmatrix} + \begin{pmatrix} 0 & 0 & 0 \\ 0 & 0 & -i\sin\omega_{23}t \\ 0 & i\sin\omega_{23}t & 0 \end{pmatrix}$$
$$= I_x\cos\omega_{23}t + (I_zI_y + I_yI_z)\sin\omega_{23}t.$$

$$\rho_L^{\Omega}(t_1) = a_1(t_1)I_{xL} + a_2(t_1)I_{yL} + a_3(t_1)I_{zL} + a_4(t_1)(I_{yL}I_{zL} + I_{zL}I_{yL}) + a_5(t_1)(I_{xL}I_{zL} + I_{zL}I_{xL}) + a_6(t_1)(I_{xL}I_{yL} + I_{yL}I_{xL}) + a_7(t_1)[3I_{zL}^2 - I(I+1)] + a_8(t_1)(I_{xL}^2 - I_{yL}^2), \quad \text{(A4)}$$

where

$$a_1(t_1) = \sin\beta\cos\beta\,[\cos\omega_{12}t_1 - (\cos^2\alpha\cos\omega_{23}t_1 + \sin^2\alpha\cos\omega_{31}t_1)],$$
$$a_2(t_1) = \sin\beta\sin\alpha\cos\alpha(\cos\omega_{31}t_1 - \cos\omega_{23}t_1),$$
$$a_3(t_1) = \cos^2\beta\cos\omega_{12}t_1 + \sin^2\beta(\cos^2\alpha\cos\omega_{23}t_1 + \sin^2\alpha\cos\omega_{31}t_1),$$
$$a_4(t_1) = \cos\beta\sin\beta(\sin^2\alpha\sin\omega_{31}t_1 - \cos^2\alpha\sin\omega_{23}t_1 - \cos 2\alpha\sin\omega_{12}t_1),$$
$$a_5(t_1) = \sin\alpha\cos\alpha\sin\beta\,[2\cos^2\beta\sin\omega_{12}t_1 + \cos 2\beta(\sin\omega_{23}t_1 + \sin\omega_{31}t_1)],$$
$$a_6(t_1) = \sin^2\beta(\sin^2\alpha\sin\omega_{31}t_1 - \cos^2\alpha\sin\omega_{23}t_1) + \cos 2\alpha\cos^2\beta\sin\omega_{12}t_1,$$
$$a_7(t_1) = \tfrac{1}{4}\cos\beta\sin^2\beta\sin 2\alpha(\sin\omega_{23}t_1 + \sin\omega_{31}t_1 - \sin\omega_{12}t_1),$$
$$a_8(t_1) = -\tfrac{1}{2}\sin 2\alpha\cos\beta\,[(1+\cos^2\beta)\sin\omega_{12}t_1 - \sin^2\beta(\sin\omega_{23}t_1 + \sin\omega_{31}t_1)]. \quad \text{(A5)}$$

In principle, any of these components of the density matrix is observable by a suitably designed detection sequence. Normally, when the field is suddenly reapplied, only the projection of the density matrix proportional to the laboratory based I_{zL} is observed. Either I_{xL} or I_{yL} can be stored along the laboratory z axis by the application of a short dc field pulse of length τ and polarized in the x–y plane prior to reapplication of the normal suddenly switched field. The second rank tensor operators must somehow be stored and transformed into first rank tensors in order to be observed. Where the sample is characterized by a distribution $P(\Omega)$, and the high field detection sequence uniformly detects all components of the density matrix contributing to I_{zL}, the high field signal must be integrated over the distribution function. In powders, where all angles α,β are equally represented, only a_3 survives the integration. For the Hamiltonian of Eq. (21),

$$-\omega_{23} = \omega_{31} = \tfrac{3}{2}\omega_D \quad \text{(A6a)}$$

and

$$\omega_{12} = 0. \quad \text{(A6b)}$$

Each angular function averages to 1/3; so the observed signal is

$$S(t_1) = \tfrac{1}{3}(1 + 2\cos\tfrac{3}{2}\omega_D t_1). \quad \text{(A7)}$$

Even in a single crystal (or otherwise ordered system, such as a liquid crystal) where the angles α and β take on a limited set of values only, all but a_1, a_3, a_4, and a_6 vanish due to the degeneracy of the Hamiltonian [Eq. (21)]. Only in ordered systems where the degeneracy of Eq. (A6a) is broken (e.g., by an asymmetry parameter in a spin-1 quadrupolar tensor, or by motional effects on a dipolar tensor) will the bulk magnetization, initially ordered along the laboratory z axis, thereafter evolve into all possible laboratory frame first and second rank tensors under the influence only of the pure zero field Hamiltonian.

For the Hamiltonian of Eq. (42), the eigenvalues have been given in Eq. (43). For a spin-1, there is no necessary degeneracy:

$$\omega_{23} = -(3+\eta)A,$$
$$\omega_{31} = (3-\eta)A, \quad \text{(A8)}$$
$$\omega_{12} = 2\eta A,$$

and each of the eight coefficients of Eq. (A4) may be nonzero in turn in ordered samples.

APPENDIX B

In this section we treat the case where the high field spectrum is sufficiently broad that pulsed NMR techniques are incapable of detecting the signal from the entire high field powder pattern, but where some portion of the high field spectrum is uniformly observed. These conditions are fulfilled if

$$\frac{3e^2qQ}{2I(2I-1)} \rightarrow \omega_1 > \frac{3}{4\omega_0}\left(\frac{e^2qQ}{2I(2I-1)}\right)^2. \quad \text{(B1)}$$

This is commonly the case for half-integral quadrupolar nuclei, where the central transition between the high field eigenstates $|-1/2\rangle \rightarrow |1/2\rangle$ is unshifted to first order by the quadrupole coupling, and the only significant signal after a resonant rf pulse of practical intensity arises from coherence between these two levels.

The approach is to repeat the calculation of Sec. II B 5, but to use as the observable not I_{zL}, but rather the actual observable $I_{xL}^{(-1/2\rightarrow 1/2)}$, i.e., transverse magnetization corresponding only to the coherence between these two levels. For small flip angles, it has been shown that the excitation of this coherence is independent of orientation in the lab-based frame.[26] Then

$$S(t_1) = \mathrm{Tr}[I_{xL}^{(-1/2\rightarrow 1/2)}\exp(-i\theta I_{yL})\rho(t_1)\exp(i\theta I_{yL})], \quad \text{(B2a)}$$

where the evolved longitudinal order stored in $\rho(t_1)$ is transformed into an observable by an rf pulse of θ degrees about the y axis. For the initial density operator $\rho(0) = I_{zL}$,

$$S(t_1) = \mathrm{Tr}[I_{xL}^{(-1/2\to 1/2)} \exp(-i\theta I_{yL}) I_{zL}(t_1) \exp(i\theta I_{yL})]. \tag{B2b}$$

It will be convenient to express all operators in a spherical tensor basis set. In the lab frame,

$$I_{xL}^{(-1/2\to 1/2)} = \sum_{n=1}^{I+1/2} a_n (T^j_{-1L} - T^j_{1L}) = \chi, \tag{B3}$$

where $j = 2n - 1$, and

$$I_{zL} = T^1_{0L} \tag{B4}$$

and

$$I_{zL}(t_1) = T^1_{0L}(t_1) = \exp(-iHt) T^1_{0L} \exp(iHt). \tag{B5}$$

It will also prove convenient to permute the operators in Eq. (B2b) so that the rf excitation is applied to the observed operator, which is orientation independent, rather than the evolved operator where its effects are strongly dependent on orientation,[26] and

$$S(t_1) = \mathrm{Tr}[\exp(i\theta I_{yL}) \chi \exp(-i\theta I_{yL}) T^1_{0L}(t_1)]. \tag{B6}$$

Focusing on the transformed operator

$$\begin{aligned}
&\exp(i\theta I_{yL}) \chi \exp(-i\theta I_{yL}) \\
&\quad = \sum_{n=1}^{I+1/2} a_n \sum_{m=-j}^{j} [d^j_{m-1}(\theta) - d^j_{m1}(\theta)] T^j_{mL} \\
&\quad = \sum_{n=1}^{I+1/2} 2a_n \sum_{m=-j}^{j} d^j_{m-1}(\theta) T^j_{mL}.
\end{aligned} \tag{B7}$$

Because the evolved operator $I_{zL}(t_1)$ corresponds to longitudinal order, only terms in the sum for $m = 0$ can contribute to the trace of Eq. (B6), and we restrict ourselves to these terms. Defining

$$b_n = 2a_n d^j_{0-1}(\theta) \tag{B8}$$

and

$$S(t_1) = \mathrm{Tr}\left[T^1_{0L}(t_1)\left(\sum_{n=1}^{I+1/2} b_n T^j_{0L}\right)\right]. \tag{B9}$$

Equation (B9) will be most readily evaluated in the molecular frame where the Hamiltonian is homogeneous. The laboratory frame and the molecular frame are related by a coordinate transformation $R(\Omega)$. For purposes of calculation, a single orientation Ω is chosen. The signal is then integrated over a powder distribution (i.e., all Ω equally probable):

$$\begin{aligned}
S(t_1) &= \int S^{\Omega}(t_1) d\Omega = \int \mathrm{Tr}\left[R\left(\sum_{n=1}^{I+1/2} b_n T^j_{0L}\right) R^{-1}\right. \\
&\quad \left. \times \exp(-iH_M t_1) R T^1_{0L} R^{-1} \exp(-iH_M t_1)\right] d\Omega \\
&= \int \mathrm{Tr}\left(\sum_{n=1}^{I+1/2} b_n \sum_{l=-j}^{j} D^j_{l0}(\Omega) T^j_{lM} \left\{\exp(-iH_M t_1)\right.\right. \\
&\quad \left.\left. \times \left[\sum_{k=-1}^{1} D^1_{k0}(\Omega) T^1_{kM}\right] \exp(iH_M t_1)\right\} d\Omega\right) \\
&= \sum_{n=1}^{I+1/2} b_n \int \sum_{l=-j}^{j} \sum_{k=-1}^{1} D^j_{l0}(\Omega) D^1_{k0}(\Omega) \\
&\quad \times \mathrm{Tr}[T^j_{lM} T^1_{kM}(t_1)] d\Omega.
\end{aligned} \tag{B10}$$

The entire angular dependence in Eq. (B10) lies in the rotation matrices (because we have assumed that the operator detected in high field is uniformly excited). Then using the well known properties of rotation matrices[76]

$$D^{*j}_{kq}(\Omega) = (-1)^{k-q} D^j_{-k-q}(\Omega) \tag{B11a}$$

and

$$\frac{\int D^{*j}_{k'q'}(\Omega) D^j_{kq}(\Omega) d\Omega}{\int d\Omega} = \frac{1}{2j+1} \delta_{jj'} \delta_{kk'} \delta_{qq'}, \tag{B11b}$$

we find the normalized, integrated signal

$$\begin{aligned}
S(t_1) &= \left\{\sum_{n=1}^{I+1/2} b_n \sum_{l=-j}^{j} \sum_{k=-1}^{1} \right. \\
&\quad \left. \times \int D^j_{l0}(\Omega) D^1_{k0}(\Omega) d\Omega \Big/ \int d\Omega \, \mathrm{Tr}[T^j_{lM} T^1_{kM}(t_1)]\right\} \\
&= b_1 \sum_{l=-1}^{1} \frac{(-1)^l}{3} \mathrm{Tr}[T^1_{-lM} T^1_{lM}(t_1)]
\end{aligned} \tag{B12a}$$

$$= \frac{b_1}{3}[I_{xM} I_{xM}(t_1) + I_{yM} I_{yM}(t_1) + I_{zM} I_{zM}(t_1)]. \tag{B12b}$$

All other terms have zero integrated intensity due to the orthogonality relation equation (B11b). The signal detected in high field is identical to that observed if the entire powder pattern were observed, to within a scaling constant

$$b_1 = \frac{3}{4I(I+1)} \sin\theta. \tag{B13}$$

For large flip angles θ, the details of the excitation and detection period t_2 become more important, because the amount of the operator $I_{zL}(t_1)$ transformed into an observable transverse magnetization becomes orientation dependent. Therefore, the integration in Eq. (B12) includes an additional Ω dependence in the detected operator, because both the effective nutation frequency under the influence of an applied rf field and the subsequent signal amplitude of the central transition depend on the magnitude of the high field value of the local fields, and therefore on Ω.[26] Only for small flip angle excitation is uniform excitation of the central transition possible. Quantifying what is meant by small flip angles, zero field spectra of half-integral quadrupolar nuclei can be observed without intensity distortion if the high field signal is measured immediately after a θ pulse, for

$$\gamma B_{\mathrm{rf}} \tau = \theta < \frac{\pi}{2(2I+1)}, \tag{B14}$$

and where τ is the length of the applied pulse and B_{rf} the strength of the rf field.[26(c)]

[1] U. Haeberlen, Adv. Magn. Reson. Suppl. 1 (1976).
[2] Z. Luz and S. Meiboom, J. Chem. Phys. 59, 275 (1973); R. Wise, D. Smith, and J. Doane, Phys. Rev. A 7, 1366 (1973); S. J. Opella and J. S. Waugh, J. Chem. Phys. 66, 4919 (1977); R. Hentschel, J. Schlitter, H. Sillescu, and H.

W. Spiess, *ibid.* **68,** 56 (1978); J. Schlitter, H. Sillescu, and H. W. Spiess, Polymer **22,** 1516 (1981); J. H. Davis, Biochim. Biophys. Acta **737,** 117 (1983).
[3]N. Bloembergen and J. A. Rowland, Acta, Metallurg. **1,** 731 (1953).
[4]G. E. Pake, J. Chem. Phys. **16,** 327 (1948).
[5]D. P. Weitekamp, A. Bielecki, D. Zax, K. Zilm, and A. Pines, Phys. Rev. Lett. **50,** 1807 (1983).
[6]N. F. Ramsey and R. V. Pound, Phys. Rev. **81,** 278 (1951).
[7]A. G. Anderson, Phys. Rev. **115,** 863 (1959); **125,** 1517 (1962).
[8]A. G. Redfield, Phys. Rev. **130,** 589 (1963).
[9](a) R. L. Strombotne and E. L. Hahn, Phys. Rev. A **133,** 1616 (1964); (b) R. E. Slusher and E. L. Hahn, Phys. Rev. **166,** 332 (1968); (c) J. Koo and Y.-N. Hsieh, Chem. Phys. Lett. **9,** 238 (1971); (d) Y. Hsieh, J. C. Koo, and E. L. Hahn, *ibid.* **13,** 563 (1972).
[10](a) R. Blinc *et al.*, J. Chem. Phys. **57,** 5087 (1972); (b) D. T. Edmonds, Phys. Rep. C **29,** 235 (1977); Int. Rev. Phys. Chem. **2,** 103 (1982); (c) L. S. Batchelder, J. Clymer, and J. L. Ragle, J. Chem. Phys. **74,** 4791 (1981); (d) C. R. Brett and D. T. Edmonds, J. Magn. Reson. **49,** 304 (1982); (e) T. L. Brown *et al.*, J. Am. Chem. Soc. **104,** 1172 (1982); (f) M. Suhara and J. A. S. Smith, J. Magn. Reson. **50,** 237 (1982); (g) I. J. F. Poplett, *ibid.* **50,** 382 (1982).
[11]W. P. Aue, E. Bartholdi, and R. R. Ernst, J. Chem. Phys. **64,** 2229 (1976).
[12](a)J. M. Millar, A. M. Thayer, A. Bielecki, D. B. Zax, and A. Pines, J. Chem. Phys. **83,** 934 (1985); (b) R. Kreis, D. Suter, and R. R. Ernst, Chem. Phys. Lett., **118,** 120 (1985).
[13]L. E. Erickson, Phys. Rev. **143,** 295 (1966); J. Schmidt and J. H. van der Waals, Chem. Phys. Lett. **3,** 343 (1969); E. R. Bernstein and G. M. Dobbs, Phys. Rev. B **11,** 4623 (1975); R. Bramley and S. J. Strach, Chem. Phys. Lett. **79,** 183 (1981); Chem. Rev. **83,** 49 (1983); J. Chem. Phys. **82,** 2437 (1985); J. Magn. Reson. **61,** 245 (1985).
[14](a) M. H. Cohen and F. Reif, Solid State Phys. **5,** 321 (1957); (b) T. P. Das and E. L. Hahn, Solid State Phys. Suppl. **1,** (1958).
[15]F. Reif and E. M. Purcell, Phys. Rev. **91,** 631 (1953).
[16](a) G. J. Enholm, J. P. Ekstrom, M. T. Loponen, and J. K. Soini, Cryogenics **19,** 673 (1979); (b) G. J. Enholm *et al.*, Phys. Rev. Lett. **42,** 1702 (1979); (c) G. J. Enholm *et al.*, J. Low Temp. Phys. **39,** 417 (1980).
[17]D. A. Shirley, S. S. Rosenblum, and E. Matthias, Phys. Rev. **170,** 363 (1968); H. Haas and D. A. Shirley, J. Chem. Phys. **58,** 3339 (1973).
[18]L. S. Batchelder and J. L. Ragle, J. Magn. Reson. **37,** 469 (1980).
[19]M. Packard and R. Varian, Phys. Rev. **93,** 941 (1954).
[20]E. L. Hahn, Phys. Rev. **80,** 580 (1950); H. Y. Carr and E. M. Purcell, *ibid.* **94,** 630 (1954).
[21]F. Bloch, Phys. Rev. **102,** 104 (1956).
[22]M. Mehring, *High Resolution NMR in Solids* (Springer, Berlin, 1983).
[23]R. A. Marino and S. M. Klainer, J. Chem. Phys. **67,** 3388 (1977); A. R. Kessel and O. S. Zueva, Phys. Lett. A **68,** 347 (1978); A. E. Mefed, Sov. Phys. Solid State **21,** 485 (1979); R. S. Cantor and J. S. Waugh, J. Chem. Phys. **73,** 1054 (1980); D. Ya. Osokin, Phys. Status. Solidi **102,** 681 (1980).
[24]J. S. Waugh, Proc. Natl. Acad. Sci. U.S.A. **73,** 1394 (1976); M. E. Stoll, A. J. Vega, and R. W. Vaughan, J. Chem. Phys. **65,** 4093 (1976); R. K. Hester, J. L. Ackerman, B. L. Neff, and J. S. Waugh, Phys. Rev. Lett. **36,** 1081 (1976); M. Linder, A. Hohener, and R. R. Ernst, J. Chem. Phys. **73,** 4959 (1980).
[25]M. Munowitz and R. G. Griffin, J. Chem. Phys. **76,** 2848 (1982); **77,** 2217 (1982); M. G. Munowitz, T. H. Huang, C. M. Dobson, and R. G. Griffin, J. Magn. Reson. **57,** 56 (1984).
[26](a) A. Samoson and E. Lippmaa, Chem. Phys. Lett. **100,** 205 (1983); (b) Phys. Rev. B **28,** 6567 (1983); (c) D. Fenzke, D. Freude, T. Frohlich, and J. Haase, Chem. Phys. Lett. **111,** 171 (1984).
[27]A. M. Portis, Phys. Rev. **91,** 1971 (1953); M. M. Maricq and J. S. Waugh, J. Chem. Phys. **70,** 3300 (1979). In the terminology of Maricq and Waugh, an "inhomogeneous" interaction is one where the Hamiltonian for that interaction (or sum of interactions) commute with itself for all orientations. Practically speaking, this is equivalent to saying that an inhomogeneous interaction has a spectrum which can be resolved into a magnitude convoluted with a lineshape function, and in principle a simulation of the powder spectrum can be made without having to explicitly calculate the spectrum at each orientation. Chemical shifts and quadrupolar couplings are examples of inhomogeneous interactions; multispin dipolar couplings, "homogeneous" interactions. Below, we will use the term homogeneous in a related but different sense.
[28]M. Bloom, J. H. Davis, and A. L. MacKay, Chem. Phys. Lett. **80,** 198 (1981); E. Sternin, M. Bloom, and A. L. MacKay, J. Magn. Reson. **55,** 274 (1983).
[29]U. Haeberlen and J. S. Waugh, Phys. Rev. **175,** 453 (1968); **185,** 420 (1969).
[30]D. B. Zax, A. Bielecki, K. W. Zilm, and A. Pines, Chem. Phys. Lett. **106,** 550 (1984).
[31]J. W. Hennel, A. Birczynski, S. F. Sagnowski, and M. Stachurowa, Z. Phys. B **56,** 133 (1984).
[32]This convention agrees with that established in Ref. 30 but not Ref. 5, where the factor 3/2 was included in the definition of ω_D and an additional factor of $1/\pi$ was incorrectly inserted.
[33]Z. Luz and S. Meiboom, J. Chem. Phys. **59,** 1077 (1973); W. S. Warren, D. P. Weitekamp, and A. Pines, *ibid.* **73,** 2085 (1980); S. W. Sinton, D. B. Zax, J. B. Murdoch, and A. Pines, Mol. Phys. **53,** 333 (1984).
[34]D. B. Zax, A. Bielecki, M. A. Kulzick, E. L. Muetterties, and A. Pines, J. Phys. Chem. (submitted).
[35](a) I. Waller, Z. Phys. **79,** 370 (1932); (b) H. Bayer, *ibid.* **130,** 227 (1951); (c) A. Abragam and K. Kambe, Phys. Rev. **91,** 894 (1953); (d) J. L. Ragle, J. Phys. Chem. **63,** 1395 (1959); (e) S. Alexander and A. Tzalmona, Phys. Rev. A **138,** 845 (1965); (f) G. W. Leppelmeier and E. L. Hahn, Phys. Rev. **141,** 724 (1966); (g) S. Vega, Adv. Magn. Reson. **6,** 259 (1973); (h) R. Sh. Loftullin and G. K. Semin, Adv. Nuc. Quad. Res. **2,** 1 (1975).
[36]R. Kubo and T. Toyabe, in *Magnetic Resonance and Relaxation*, edited by R. Blinc (North–Holland, Amsterdam, 1967), p. 810.
[37]R. S. Hayano *et al.*, Phys. Rev. B **20,** 850 (1979); M. Celio and P. F. Meier *ibid.* **27,** 1908 (1983); E. Holzchuh and P. F. Meier, *ibid.* **29,** 1129 (1984).
[38]Y. Wang, G. D. Stucky, and J. M. Williams, J. Chem. Soc. Perkin Trans. II **1973,** 35; J. D. Becker, D. Suwelack, and M. Mehring, Solid State. Commun. **25,** 1145 (1978); M. Mehring and J. D. Becker, Phys. Rev. Lett. **47,** 366 (1981).
[39]E. R. Andrew and R. Bersohn, J. Chem. Phys. **18,** 159 (1950); H. S. Gutowsky and G. E. Pake, *ibid.* **18,** 162 (1950); J. G. Powles and H. S. Gutowsky, *ibid.* **23,** 1692 (1953).
[40](a) A. Abragam and W. G. Proctor, Phys. Rev. **109,** 1441 (1958); (b) *Principles of Nuclear Magnetism* (Clarendon, Oxford, 1982).
[41]A. Pines, M. G. Gibby, and J. S. Waugh, J. Chem. Phys. **59,** 569 (1973).
[42]D. P. Weitekamp, J. R. Garbow, and A. Pines, J. Chem. Phys. **77,** 2870 (1982); L. Braunschweiler and R. R. Ernst, J. Magn. Reson. **53,** 521 (1983); P. Caravatti, L. Braunschweiler, and R. R. Ernst, Chem. Phys. Lett. **100,** 305 (1983).
[43]A. Bielecki, J. B. Murdoch, D. P. Weitekamp, D. B. Zax, K. W. Zilm, H. Zimmerman, and A. Pines, J. Chem. Phys. **80,** 2232 (1984).
[44](a) D. T. Edmonds, M. J. Hunt, and A. L. MacKay, J. Magn. Reson. **11,** 77 (1973); (b) **20,** 505 (1975); (c) D. T. Edmonds and A. A. L. White *ibid.* **31,** 149 (1978); (d) I. J. F. Poplett and J. A. S. Smith, J. Chem. Soc. Faraday Trans. 1 **74,** 1077 (1978); (e) I. J. F. Poplett, Adv. Nucl. Quad. Reson. **4,** 115 (1980).
[45]R. G. Barnes, Adv. Nucl. Quad. Reson. **1,** 335 (1974).
[46]A. Bielecki, D. B. Zax, K. W. Zilm, and A. Pines, Rev. Sci. Instrum. (submitted).
[47]M. Alla, R. Eckman, and A. Pines, Chem. Phys. Lett. **71,** 148 (1980); D. Suter and R. R. Ernst, Phys. Rev. B **25,** 6038 (1982); C. Ye, R. Eckman, and A. Pines, J. Magn. Reson. **55,** 238 (1983).
[48]E. P. Wigner, *Group Theory and its Application to the Quantum Mechanics of Atomic Spectra* (Academic, New York, 1959).
[49]E. Brun and B. Derighetti, Helv. Phys. Acta **34,** 383 (1961).
[50]M. H. Cohen, Phys. Rev. **96,** 1278 (1954).
[51]D. B. Zax, A. Bielecki, A. Pines, and S. W. Sinton, Nature **312,** 351 (1984).
[52]R. W. G. Wyckoff, *Crystal Structures* (Wiley, New York, 1965) Vol. 3, p. 872; W. G. Segleken and H. C. Torrey, Phys. Rev. **98,** 1537 (1955).
[53]R. Kubo, Nuovo Cimento Suppl. **6,** 1063 (1957); R. A. Sack, Mol. Phys. **1,** 163 (1958).
[54]R. P. Mason, C. F. Polnaszek, and J. H. Freed, J. Phys. Chem. **78,** 1324 (1974); S. Alexander, A. Baram, and Z. Luz, Mol. Phys. **27,** 441 (1974); H. W. Spiess, Chem. Phys. **6,** 217 (1974); H. W. Spiess, R. Grosescu, and U. Haeberlen, *ibid.* **6,** 226 (1974); A. Baram, Z. Luz, and S. Alexander, J. Chem. Phys. **64,** 2231 (1976); A. Baram, *ibid.* **71,** 2503 (1979); D. E. Wemmer, D. J. Ruben, and A. Pines, J. Am. Chem. Soc. **103,** 281 (1981); H. W. Spiess and H. Sillescu, J. Magn. Reson. **42,** 381 (1981); D. Rice *et al.*, J. Am. Chem. Soc. **103,** 7707 (1981).
[55]J. W. Emsley, J. C. Lindon, and J. Tabony, Mol. Phys. **26,** 1499 (1973); P. Diehl, M. Reinhold, and A. S. Tracey, J. Magn. Reson. **19,** 405 (1975); S. Hsi, H. Zimmerman, and Z. Luz, J. Chem. Phys. **69,** 4126 (1978).
[56](a) S. Ketudat and R. V. Pound, J. Chem. Phys. **26,** 708 (1957); (b) T. Chiba, *ibid.* **39,** 947 (1963); (c) G. Soda and T. Chiba, *ibid.* **50,** 439 (1969); (d) B. H. Meier, F. Graf, and R. R. Ernst, *ibid.* **76,** 767 (1982).
[57]J. M. Millar, A. M. Thayer, A. Bielecki, D. B. Zax, and A. Pines, J. Magn. Reson. (submitted).
[58]J. Schaefer, E. O. Stejskal, R. A. McKay, and W. T. Dixon, J. Magn.

Reson. **57,** 85 (1984).
[59]A. G. Redfield, W. Fite, and H. E. Bleich, Rev. Sci. Instrum. **39,** 710 (1968); K. Hallenga and S. H. Koenig, Biochemistry **15,** 4255 (1975); R. D. Brown III, C. F. Brewer, and S. H. Koenig, *ibid.* **16,** 3883 (1977); M. Stohrer and F. Noack, J. Chem. Phys. **67,** 3729 (1977); G. Nagel, W. Woelfel, and F. Noack, Isr. J. Chem. **23,** 380 (1983); R. G. Bryant and M. Jarvis, J. Phys. Chem. **88,** 1323 (1984); C. F. Polnaszek and R. G. Bryant, J. Chem. Phys. **81,** 4308 (1984); S. H. Koenig and R. D. Brown III, J. Magn. Reson. **61,** 426 (1985).
[60]I. Solomon, Phys. Rev. **110,** 61 (1958); P. Mansfield, Phys. Rev. A **137,** 961 (1965).
[61](a) J. S. Waugh, L. M. Huber, and U. Haeberlen, Phys. Rev. Lett. **20,** 180 (1968); (b) W.-K. Rhim, D. D. Elleman, and R. W. Vaughan, J. Chem. Phys. **59,** 3740 (1973); (c) D. P. Burum and W.-K. Rhim, *ibid.* **71,** 944 (1979); (d) D. P. Burum, M. Linder, and R. R. Ernst, J. Magn. Reson. **44,** 173 (1981).
[62]E. D. Ostroff and J. S. Waugh, Phys. Rev. Lett. **16,** 1097 (1966); W.-K. Rhim, D. P. Burum, and D. D. Elleman, *ibid.* **37,** 1764 (1976); D. Suwelack and J. S. Waugh, Phys. Rev. B **22,** 5110 (1980); M. M. Maricq, *ibid.* **25,** 6622 (1982).
[63]A. Bax, N. M. Szeverenyi, and G. E. Maciel, J. Magn. Reson. **52,** 147 (1983); N. Szeverenyi, A. Bax, and G. E. Maciel, *ibid.* **61,** 440 (1985).
[64]J. Jeener, B. H. Meier, P. Bachmann, and R. R. Ernst, J. Chem. Phys. **71,** 4546 (1979); B. H. Meier and R. R. Ernst, J. Am. Chem. Soc. **101,** 6441 (1980); A. Kumar, R. R. Ernst, and K. Wuthrich, Biochem. Biophys. Res. Commun. **95,** 1 (1980); S. Macura and R. R. Ernst, Mol. Phys. **41,** 95 (1980); G. Wider *et al.*, J. Magn. Reson. **56,** 207 (1984).
[65]R. O. Day, N. Hadipour, and J. L. Ragle, J. Magn. Reson. **57,** 369 (1984); **59,** 373 (1984).
[66]A. M. Thayer, J. M. Millar, A. Bielecki, D. B. Zax, and A. Pines, J. Magn. Reson. (submitted).
[67]A. G. Redfield, Phys. Rev. **98,** 1787 (1955); C. P. Slichter and W. C. Holton *ibid.* **122,** 1701 (1961); J. Jeener and P. Brokaert, *ibid.* **157,** 232 (1967).
[68]M. Goldman, *Spin Temperature and Nuclear Magnetic Resonance in Solids* (Clarendon, Oxford, 1970).
[69]V. S. Grechishkin, V. P. Anferov, and N. Ja. Sinjavsky, Adv. Nucl. Quad. Reson. **5,** 1 (1984).
[70]T. Sleator, E. L. Hahn, C. Hilbert, and J. C. Clarke, Phys. Rev. Lett. (submitted).
[71]C. Hilbert, J. C. Clarke, T. Sleator, and E. L. Hahn, Appl. Phys. Lett. (to be published).
[72]C. D. Makowka, C. P. Slichter, and J. H. Sinfelt, Phys. Rev. Lett. **49,** 379 (1982); C. D. Makowka, C. P. Slichter, and J. H. Sinfelt, Phys. Rev. B **31,** 5663 (1985).
[73]T. M. Duncan, J. T. Yates, Jr., and R. W. Vaughan, J. Chem. Phys. **71,** 3129 (1979); T. M. Duncan, P. Winslow, and A. T. Bell, Chem. Phys. Lett. **102,** 163 (1982); S. L. Rudaz *et al.*, Phys. Rev. Lett. **54,** 71 (1985).
[74]C. J. F. Broer, Physica **10,** 801 (1943); A. Wright, Phys. Rev. **76,** 1826 (1949).
[75](a) S. Vega and A. Pines, J. Chem. Phys. **66,** 5624 (1977); (b) A. Wokaun and R. R. Ernst, *ibid.* **67,** 1753 (1977); (c) S. Vega, *ibid.* **68,** 5518 (1978).
[76]M. E. Rose, *Elementary Theory of Angular Momentum* (Wiley, New York, 1967).